S1Enhanced FcγRIII/CD16 activation by discrete ligands as independent correlates of disease severity in COVID-19 patients

Jakob Ankerhold[1,2,11] & Sebastian Giese[1,2,11] & Philipp Kolb[1,2,11], Andrea Maul-Pavicic[3,4], Nathalie Göppert[1,2], Kevin Ciminski[1,2], Clemens Kreutz[5], Achim Lother[6,7], Ulrich Salzer[3], Wolfgang Bildl[8], Tim Welsink[9], Nils G. Morgenthaler[9], Andrea Busse Grawitz[10], Daniela Huzly[1,2], Martin Schwemmle[1,2], Hartmut Hengel[1,2,12], Valeria Falcone[1,2,12]

[1]Institute of Virology, University Medical Center, Albert-Ludwigs-University Freiburg, Hermann-Herder-Str. 11, 79104 Freiburg, Germany
[2]Faculty of Medicine, Albert-Ludwigs-University Freiburg, 79104 Freiburg, Germany
[3]Department of Rheumatology and Clinical Immunology, Medical Center-University of Freiburg, Faculty of Medicine, University of Freiburg, Hugstetterstr. 55, 79106 Freiburg, Germany
[4]Center for Chronic Immunodeficiency (CCI), Medical Center-University of Freiburg, Faculty of Medicine, University of Freiburg, Breisacherstr. 115, 79106 Freiburg, Germany
[5]Institute of Medical Biometry and Statistics, Faculty of Medicine and Medical Center, University of Freiburg, Stefan Meier Str. 26, 79104 Freiburg, Germany
[6]Heart Center Freiburg University, Department of Cardiology and Angiology I, Faculty of Medicine, University of Freiburg, Hugstetterstr. 55, 79106 Freiburg, Germany
[7]Institute of Experimental and Clinical Pharmacology and Toxicology, Faculty of Medicine, University of Freiburg, Albertstr. 25, 79104 Freiburg, Germany
[8]Institute of Physiology II, Faculty of Medicine, University of Freiburg, Hermann-Herder-Str. Freiburg, Germany
[9]InVivo BioTech Services GmbH, 16761 Hennigsdorf, Germany
[10]Institute of Clinical Chemistry and Laboratory Medicine, Medical Center - University of Freiburg, Faculty of Medicine, University of Freiburg, Hugstetterstr. 55, 79106 Freiburg, Germany
[11]contributed equally
[12]corresponding authors

One sentence summary

Severity of disease in COVID-19 patients is associated with enhanced CD16 activation by afucosylated S-specific IgG and CD16-reactive circulating IgG-complexes.

Abstract

A dysregulated immune response with high levels of SARS-CoV-2 specific IgG antibodies is a common and distinctive feature of severe or critical COVID-19. Although a robust IgG response is typically considered to be beneficial, an overshooting activation mediated by immune receptors recognizing the Fc part of IgG (FcγRs) is thought to be detrimental and associated with immunopathology. However, direct evidence of FcγR driven immunopathology in COVID-19 is still sparse. Here, we used a cell-based FcγR activation reporter system to systematically analyze SARS-CoV-2 specific IgG responses and IgG-mediated FcγRIII (CD16) activation profiles in COVID-19 patient cohorts categorized by severity of disease. We found that increased CD16 activation by SARS-CoV-2 specific IgG is associated with a known pro-inflammatory IgG modification, namely afucosylation. Further, we identified CD16-reactive soluble IgG immune complexes (sICs) to be present in the serum of COVID-19 patients and show that the resulting CD16 activation by sICs is strongly related to disease severity. Our results provide evidence that CD16 activation by pro-inflammatory SARS-CoV-2 specific IgG together with circulating sICs is a major contributor to COVID-19 immunopathology. These findings highlight the importance of FcγR driven immunopathology in COVID-19. Further, our data highly warrant the development of targeted intervention strategies against IgG driven immunopathology following SARS-CoV-2 infection.

Introduction

Since the emergence of SARS-CoV-2 in late December 2019[1], more than 178 million laboratory confirmed infections (as of June 21, 2021) have been reported, with cases continuously rising[2]. Accordingly, rapid insights into the disease manifestations and pathogenesis have been globally obtained. A hallmark of the coronavirus disease 2019 (COVID-19) is a respiratory infection which can progress to an acute respiratory distress syndrome (ARDS). Next to asymptomatic infections, COVID-19 symptoms differ widely according to the disease process and may comprise fever, coughing, pneumonia, dyspnea, hypoxia and lymphopenia[3]. While fever and coughing are common symptoms, pneumonia, hypoxia, dyspnea, certain organ manifestations and lymphopenia indicate critical or fatal infections. Pronounced dyspnea can eventually progress to ARDS, a severe complication frequently observed in critically ill patients[4]. Although disease severity and in particular breathing difficulties are related to viral load[5], age[6-8] and underlying medical conditions[7,8], the kinetics of respiratory failure strongly suggests an essential role of the host immune response[3,7]. Typically, aggravation occurs between 9-12 days after symptom onset[8] and correlates with high levels of SARS-CoV-2 specific IgG antibodies and systemic effects of pro-inflammatory cytokines such as IL-6 and TNFα[3,9,10]. This cytokine release, primarily the result of macrophage and T helper (T_H) cell activation[11], includes pattern recognition receptor (PRR) signaling in the context of innate immunity but also Fcγ receptor (FcγR) activation[12]. Triggered by immune complexes (antibody-antigen complex), the cytokine release following FcγR activation represents a potent defense mechanism against invading pathogens. A prototypical activating FcγR in this regard is FcγRIII (CD16) expressed by NK cells and monocyte-derived macrophages (CD16A)[13] or neutrophils (CD16B, 98% sequence identical ectodomains). Specifically, CD16 is able to recognize circulating soluble immune complexes (sICs) as they are formed in certain autoimmune diseases such as lupus[14-17] and viral infections[18]. Overstimulation of activating FcγRs in these cases is associated with disease severity[18-20] and thus an FcγR-driven overshooting inflammatory response[12] might be an explanation for the pronounced immunopathology observed during severe courses of COVID-19[21]. Consistently, hyper-inflammation in SARS-CoV-1 and MERS infected patients has been previously proposed as a possible pathogenic factor[22] and could be demonstrated in mice and macaques infected with SARS-CoV-1[23,24]. Furthermore, N297-dependent glycan-modifications such as afucosylation within the constant region of SARS-CoV-2 specific IgG antibodies enhance binding to FcγRs, in turn driving inflammation. Enhanced FcγR activation by low-fucosylated anti-SARS-CoV2-S IgG leading to excessive alveolar macrophage activation has specifically been shown to drive severe COVID-19 disease progression[25].

Therefore we aimed to delineate the contribution of IgG-mediated effector functions regarding COVID-19 severity in patient cohorts with various severity of SARS-CoV-2 infection. We monitored antigen-specific IgG responses in patients with mild, critical and severe COVID-19 disease with regard to titer, kinetics and CD16 activation. This revealed a marked correlation between CD16 activation by patient IgG and severity of disease. Additionally, we identified circulating sICs to be abundantly present in the serum of critically and severely diseased patients, but not in the serum of those with a mild disease. As sIC-mediated CD16 activation independently correlates with disease severity, we provide evidence that also sIC formation is indicative of disease progression. Our findings enable new avenues of intervention against COVID-19 and highly warrant further investigation into the origin and composition of sICs in COVID-19 disease.

Results

Patients and clinical information.

We retrospectively analyzed serial serum samples collected for routine diagnostic testing from 41 patients hospitalized at our tertiary care center between March and June 2020 with SARS-CoV-2 infection confirmed by real-time PCR. Based on the clinical course, we categorized patients as either severely diseased (hospitalized with COVID-19 related pneumonia) versus critically diseased (COVID-19 related pneumonia and eventually in need of invasive mechanical ventilation). In total, 27 patients with critical and 14 with severe courses of disease were grouped into separate cohorts (Table 1). Most patients were older than 60 years with an overall mean age of 68 years (63 years and 76 years in the critically and severely diseased patients respectively).

The majority of patients in both groups had comorbidities of different origin with cardiovascular diseases including hypertension representing the most frequent pathology (35/41, 85%). Similar to previous reports, high Interleukin 6 (IL-6) and C-reactive protein (CRP) levels were associated with severity of disease (Ø IL-6: 1452.1 pg/ml in the critical group vs 46.1 pg/ml in the severe group and Ø CRP: 162.2 mg/l vs 65.3 mg/l Ø13-25 days post symptom onset respectively). Similarly, procalcitonin, a biomarker of microbial coinfection, was significantly higher in critically diseased patients (Ø value 9.9 ng/ml vs 0.17 ng/ml). Bacterial superinfection represented a further complication in 39% of the patients and was only slightly more frequent in patients with critical disease (11/27, 41% vs 5/14, 33%). More than half of the patients (59%) were treated with hydroxycloroquine/Kaletra®, (18/27, 67% in the

critical group vs 6/14, 43% in the severe group). Notably, at the time of serum acquisition, only one patient received steroid treatment, which was given due to underlying chronic obstructive pulmonary disease. Finally, mortality rate was 37% (10/27) in critically and 7% (1/14) in severely diseased patients.

Kinetics of IgG antibody responses following symptom onset across severe and critical courses of disease.

It has been proposed that elevated SARS-CoV-2 antibody titers are associated with disease severity[10] and may play a role not only in the clearance but also in the pathogenesis of SARS-CoV-2 infection[26]. We therefore initially analyzed the levels and kinetics of SARS-CoV-2 specific IgG in serial serum samples from patients hospitalized with critical (n=27) or severe (n=14) illness, a setting we also used in the following experiments. A total of 125 (critically diseased) and 79 (severely diseased) serum samples, obtained from the aforementioned patients at different time points within 6-25 days following symptom onset were analyzed by commercially available S1- and N- specific ELISA-based assays. Assay specificity was confirmed analyzing healthy donor (HD) serum samples (n=30) as negative control (Figure 1-figure supplement 1 A, B). Most patients developed detectable SARS-CoV-2 specific IgG responses within 9-14 days after symptom onset. SARS-CoV-2 specific IgG gradually increased over time in both severely and critically diseased patients reaching a plateau at 18-20 days after symptom onset (Figure 1 A, B). Varying antibody response kinetics were observed for each individual patient (Figure 1-figure supplement 2 A-D) with anti-N IgG titers rising significantly earlier than anti-S1 IgG (12.5 days ± 3.3 days vs 10.6 ± 3.8; p= 0.0091). A trend towards earlier seroconversion for anti-S1 IgG could be observed in critically diseased patients (mean time of seroconversion 11.4 ± 3.0 days in critically diseased patients vs 12.9 ± 3.8 days for severely diseased patients; p = 0.24), whereas time of seroconversion for anti-N IgG was similar in both groups (10.1 ± 3.2 and 10.4 ± 4.2 days for critically and severely diseased patients, respectively; p = 0.83). S1- and N-specific IgG levels at plateau did not significantly differ between the two groups. No significant difference between deceased and discharged patients was measured 13-25 days after symptom onset (Figure 1- figure supplement 1 C, D, E). Next, we evaluated and compared the neutralizing capacity of SARS-CoV-2 IgG in either critically versus severely diseased patients in a plaque-reduction assay (Figure 1 C). All patients mounted a robust neutralizing antibody response (91% ± 10.5 % neutralization at a 1:64 serum dilution), with peaking titers at 18-20 days following symptom onset. Of note, two critically diseased patients developed a neutralizing response already at 6-8 days after symptom onset. In

160 summary, we observed only minor differences in cohort wide kinetics of S1- or N- specific IgG
161 levels between patients hospitalized with severe or critical clinical courses indicating that
162 antibody levels per se did not correlate with severity of disease in our study.
163
164 **Patients with severe COVID 19 show enhanced CD16 activation by S-specific IgG**
165 **antibodies.**
166 FcγRIII (CD16) activation initiates multiple protective effector functions such as antibody-
167 dependent cellular cytotoxicity (ADCC) by natural killer (NK) cells as well as antibody-
168 dependent cytokine and chemokine secretion by NK cells and macrophages[12,27]. However,
169 excessive FcγR stimulation can have severe adverse effects such as elevated cytokine release
170 as observed in autoimmune diseases or viral infections[12]. Therefore, we hypothesized that an
171 exaggerated FcγR mediated activation triggered by SARS-CoV-2 specific IgG might contribute
172 to the exacerbation of COVID-19 in severely compared to critically diseased patients. To
173 address this, we analyzed the ability of SARS-CoV-2 specific antibodies to activate CD16
174 (158V) using a previously established cell-based reporter system[28] (Figure 2- figure supplement
175 1A). Considering the typically late time point of health deterioration, we performed an analysis
176 of CD16 activation triggered by SARS-CoV-2 specific IgG on serum samples obtained 13-25
177 days following symptom onset (Figure 2). Sera were analyzed at a 1:500 dilution to stay within
178 the dynamic range of detection (Figure 2- figure supplement 2). Depending on the availability
179 of sample material 2-8 samples/patient/time-point were included in this analysis. If available in
180 sufficient quantity, sera were reanalyzed. Reproducibility was tested using available serum
181 surplus (Figure 2- figure supplement 3). Sera from 28 patients with mild SARS-CoV-2 infection
182 and 30 healthy blood donors were included for reference. Semi-quantitative assessment of IgG
183 titers using antigen-specific ELISA revealed comparable levels between critically and severely
184 diseased patient cohorts (Figure 2 A, B, C). In contrast, S- ($p=0.0147$) and RBD-specific
185 ($p=0.0120$) but not N-specific IgG-mediated CD16 activation was significantly increased in
186 critically compared to severely diseased patients (Figure 2 D-F). Furthermore, normalizing
187 CD16 activation to antigen-specific IgG titers, revealed significantly stronger CD16 activation
188 by S- ($p=0.0033$) and N-specific ($p=0.006$) IgG compared to mildly diseased patients (Figure 2
189 G-I). Intriguingly, we observed a heterogeneous CD16 activation pattern characterized by either
190 high or low CD16-activating sera irrespective of the clinical manifestation (Figure 2 D-F).
191 Overall, a significant positive correlation could be determined between anti-SARS-CoV-2
192 antigen IgG titers and CD16 activation (Figure 2-figure supplement 4). Our data document a
193 sustained CD16 activation by SARS-CoV-2 specific antibodies particularly in patients

194 suffering from critical COVID-19 disease. Based on these results we confirmed the notion that
195 elevated FcγRIII activation by S- and or RBD-specific IgG might contribute to disease severity
196 of COVID-19.
197
198 **Enhanced Fcγ-afucosylation of S-specific IgG in critically and severely diseased patients**
199 **results in increased CD16 activation.**
200 We speculated that differences in Fcγ mediated effector functions might contribute to disease
201 severity of COVID-19 and thus compared CD16 high- versus CD16 low-activating patient sera
202 regarding their SARS-CoV-2 specific IgG core fucosylation. Inspired by previous findings[29-31]
203 we focused on determining IgG core fucosylation of S- and N- specific SARS-CoV2 IgG. To
204 determine IgG core fucosylation we adapted a lectin-based ELISA preceded by antigen-specific
205 antibody purification from immobilized SARS-CoV-2-antigen. Analysis of anti-S and anti-N
206 IgG core fucosylation was performed on serum pools containing five sera of either critically or
207 severely diseased patients obtained 13-25 days post symptom onset. Given the aforementioned
208 heterogeneity in CD16-activation, we analyzed pools of 5 sera of either critically or severely
209 diseased patients characterized by either high or low CD16-activation.To stay within the
210 dynamic detection range, relative fucosylation was analyzed at a dilution of 1:4 (Figure 3).
211 When analyzing serum pools from critically and severely diseased patients we determined a
212 significantly lower level of core fucosylation among the high CD16 activators (Figure 3, plain-
213 colored bars) compared to the low CD16 activators (Figure 3, shaded bars). This applied for
214 both the S- and N-specific antibodies. These results are in line with previously published
215 findings regarding the effect of Fcγ-afucosylation on CD16 effector functions[29,32] and
216 recapitulate similar findings in the context of COVID-19[30,31]. However, we did not observe
217 significant differences between critically and severely diseased patients.
218
219 **COVID-19 disease severity correlates with an increase in CD16-reactive soluble IgG**
220 **complexes.**
221 Next to afucosylation, it has been proposed that uncleared antigen-antibody immune complexes
222 (ICs) might further exacerbate inflammation, explaining complications observed in COVID-19
223 such as cytokine storm, systemic vasculitis, microvascular thrombosis and organ failure[33-35].
224 However, the presence of circulating, soluble ICs (sICs) in critically or severely diseased
225 patients has not been conclusively shown yet. As extensive FcγR activation by sICs might
226 contribute to the severe systemic inflammatory state occurring in some COVID-19 patients with
227 prolonged disease, we surmised that sICs might be a putative explanation for the marked

228 differences in IL-6, PCT and CRP levels between critically and severely diseased patients
229 (Table 1). We thus set out to characterize our patient cohort regarding the presence of sICs in
230 serum samples taken at various time points during disease and after hospitalization. To this end,
231 we deployed a novel cell-based reporter assay developed to quantify CD16 (158V) activation
232 by IgG-containing sICs[17]. As recently shown, the assay does not react to monomeric IgG or
233 small dimeric complexes in solution, but specifically identifies multimeric sICs and has been
234 successfully used to identify sICs in patients with systemic lupus erythematosus (SLE)[16].
235 Moreover, the assay is sensitive to sICs size with larger complexes leading to stronger receptor
236 activation compared to small complexes. Analysis of serum samples, obtained 13-25 days after
237 symptom onset, revealed the presence of highly CD16-reactive sICs in SARS-CoV-2 infected
238 patients compared to healthy individuals (Figure 4A). Next, we compared sIC-mediated CD16
239 activation between COVID-19 patients of varying disease severity. While all COVID-19
240 patient groups tested positive for reactive sICs compared to healthy control (HD) sera, we found
241 that critically diseased patients show a striking increase in reactive sICs compared to patients
242 with severe or mild disease (Figure 4B). Only 6 out of 27 patients with critical disease (22%)
243 showed no sIC-mediated CD16 activation. As we did not detect reactive sICs in the serum of
244 47 patients with acute respiratory distress syndrome (ARDS; mean age 57.5 years) in response
245 to infections of different etiology including CMV reactivation, HIV, influenza or TBC
246 infection, we conclude that the formation of reactive sICs is associated with severe SARS-CoV-
247 2 disease (Figure 4-figure supplement 1). Longitudinal analysis of reactive sICs in the serum
248 of critically or severely diseased patients revealed high CD16 activation levels in 4 critically
249 diseased patients already 6 to 8 days after symptom onset (Figure 4C). Of note, 2 of 4 patients
250 with an early increase of circulating reactive sIC eventually died. sIC-mediated CD16 activation
251 persisted in 14 of 19 critically diseased patients at high levels until day 26 after symptom onset.
252 sIC-mediated CD16 activation in severely diseased patients was slightly delayed compared to
253 critically diseased patients and was first detected in 4 patients 9-11 days after symptom onset
254 (Figure 4C). Only 4 of 14 patients with severe disease showed detectable sIC-mediated CD16
255 activation. To verify that sICs represent the CD16-reactive component in the serum of COVID-
256 19 patients, we analyzed serum-mediated CD16 activation before and after PEG8000-
257 precipitation. This treatment was previously shown to selectively precipitate large IgG
258 complexes from solution[36]. For this analysis, pools of 8 sera, showing either high (IC+) or no
259 (IC-) CD16 activation, were compared. Sera from healthy donors (HD) served as a negative
260 control. Compatible with the hypothesis of serum-derived sICs driving CD16 activation, no
261 activation was observed following incubation with 3.5% PEG8000 (Figure 4-figure supplement

262 2 A). To ensure, that the treatment did not precipitate monomeric IgG, we tested the depleted
263 sera for remaining S1- and N-specific IgG. As depicted S1- and N- specific IgG could still be
264 detected at high levels in samples treated with 3.5% PEG8000 (Figure 4-figure supplement 2
265 B). When resolving sIC-mediated CD16 activation over the complete time of hospitalization
266 for select patients from which samples at different time points were available, we observed that
267 sIC reactivity follows a similar course as anti-S1 IgG titers in ELISA (Fig. 4-figure supplement
268 3). While this might imply that sIC formation involves SARS CoV-2 S1 antigen, we were not
269 able to identify any SARS-COV-2-derived antigens in PEG8000-precipitated sICs using
270 tandem mass spectrometry (data not shown). To further exclude the formation of multimeric
271 sICs formed from circulating S1 antigen, we also specifically targeted S1 for precipitation from
272 patient serum using biotinylated S1-specific monoclonal antibodies. However and in line with
273 our previous approach, S1-specific precipitation using streptavidin-sepharose beads and
274 subsequent mass spectrometry analysis for any SARS-CoV-2-specific antigens in sICs
275 remained inconclusive (data not shown). Recently, the role of neutrophil mediated intravascular
276 NETosis was found to play a critical role in thrombose formation and subsequent organ damage
277 observed in severe clinical forms of COVID-19[37]. Since this process could mediate the
278 formation of aggregated IgG as a form of sICs, we next tested whether Benzonase® nuclease
279 treatment of patient serum would dissolve reactive sICs. To this end we tested sera from
280 critically diseased patients or healthy individuals and compared CD16 reactivity before and
281 after nuclease treatment (Figure 4-figure supplement 4). Nuclease activity in diluted human
282 serum was controlled using plasmid DNA for reference. This revealed that nucleic acid was not
283 involved in the formation of CD16-reactive sICs in critically diseased patients. Finally, we
284 tested pooled patient sera for autoantibodies against a panel of prototypical autoantigens
285 associated with autoimmune disease including anti-nuclear autoantibodies (ANA) by indirect
286 immunofluorescence, dsDNA autoantibodies by ELISA and autoantibodies against the
287 extractable nuclear antigens (nRNP/Sm, Sm, SS-A, Ro-52, SS-B, Scl-70, PM-Scl, Jo-1, CENP
288 B, PCNA, nucleosomes, histones, ribosomal P-protein, AMA-M2, DFS70) by dot blot in case
289 SARS-CoV-2 infection triggers autoantibody formation and possible sIC formation. However,
290 no significant autoantibody titers could be detected in any sera pool (data not shown). Although
291 we were not able to identify their origin, our data clearly indicates the presence of circulating
292 sICs in COVID-19 patients with an increase in CD16-reactive sICs corresponding with severity
293 of disease. Accordingly, we conclude that circulating sICs are a hitherto unknown, yet
294 contributing factor to COVID-19 disease severity and, regarding infectious diseases, our
295 findings represent an observation unique to severely diseased COVID-19 patients.

296 **Discussion**

297 We collected and analyzed data from 41 COVID-19 patients hospitalized at the University
298 Hospital Freiburg. Patients were categorized by severity of disease into severely (n=14) and
299 critically diseased patients (n=27). Both groups were of comparable average age and had a
300 similar male-to-female ratio. For comparison we also analyzed 28 mildly diseased and 30
301 healthy individuals. As key findings we identify the potential of *de novo* produced SARS-CoV-
302 2 IgG and the presence of soluble immune complexes activating FcγRIII/CD16 as independent
303 risk factors closely associated with severe courses of COVID-19.

304

305 **CD16 activation by SARS-CoV-2 specific IgG is increased in critically diseased patients.**

306 FcγR activation by anti-viral IgG represents a potent defense mechanism, directing the immune
307 response to the site of viral replication[38-41]. However, persistent infection can lead to prolonged
308 stimulation of FcγRs, driving an overshooting and potentially damaging inflammatory
309 response[12,18]. A potential key component in prolonged inflammation following SARS-CoV-2
310 infection is FcγR mediated cytokine and chemokine release by several immune cells as their
311 activation has been implied in severity of disease[29,31,42]. Along these lines, glycan profiles of
312 anti-SARS-CoV2 IgG have been identified as major correlates of COVID-19 disease
313 progression[29-31]. As these modifications particularly affect CD16 activation, we characterized
314 our patient groups with regard to CD16 activation by S- and N-specific IgG and determined
315 significantly increased CD16 activation by S, N and RBD specific IgG in sera from severely
316 and critically diseased patients compared to mildly diseased patients. We further identified a
317 higher level of afucosylation being indicative of COVID-19 severity, which is in line with
318 previous studies[29-31], and now directly link this general observation to an increased CD16
319 activation. Taken together, we find that CD16 activation by SARS-CoV-2-specific IgG can be
320 directly correlated to IgG glycan modifications and disease severity.

321

322 **Circulating sICs contribute to COVID-19 disease severity**

323 Based on the herein presented results identifying CD16 activation to be a major correlate of
324 disease severity, we further explored this using an adapted FcγR activation assay optimized to
325 measure soluble immune complexes (sICs)[17]. Indeed, we provide first evidence of such
326 circulating sICs in the serum of COVID-19 patients and experimentally confirm previous
327 hypotheses suggesting immune complexes as potential drivers of disease progression in
328 COVID-19[33-35]. In fundamental contrast to opsonized antigens decorating virus-infected cells,

329 sICs become distributed systemically. Thus constitutive activation of CD16^{+} monocytes,
330 granulocytes and NK cells could readily explain systemic responses which potentiate local
331 inflammation in virus-infected tissues intensifying organ damage and dysfunction. Although
332 the origin of the circulating immune complexes still remains elusive, we clearly show that the
333 presence of IgG-containing sICs is restricted to SARS-CoV-2 infection and that complexed IgG
334 is directly responsible and sufficient for the observed CD16 activation by patient serum. As we
335 find sIC reactivity to roughly follow SARS-CoV2-S specific IgG responses, we speculated that
336 circulating S or shed S1-antigens might still be involved in sIC formation, albeit in a form we
337 were not able to detect. In support of this hypothesis, it has recently been published that
338 circulating S-antigen can be detected in the plasma of individuals who received two doses of
339 the mRNA-1273 (Moderna) vaccine[43]. S1 shedding was also reported to play a role in virion
340 infectivity as the introduction of a D614G mutation significantly enhanced infectivity due to an
341 increased S-protein density in the virion[44]. Finally, others have identified potential mechanisms
342 leading to S-antigen shedding in viral infection and proposed a link between the presence of
343 circulating S-antigen and disease severity[45]. Alternatively, IgG auto-antibodies of diverse
344 specificity might cause the formation of the CD16 triggering sICs we herein identified. In fact,
345 several studies have described that auto-antibodies can be frequently detected in critically ill
346 COVID-19 patients[46-48]. In particular, very recent work shows that an acute SARS-CoV-2
347 infection triggers the *de novo* IgG production against multiple autoantigens. Interestingly, 60-
348 80% of all hospitalized COVID-19 patients had anti-cytokine IgG (ACA)[49]. The authors show
349 that ACA levels and specificity change over time during hospitalization, suggesting ACA
350 induction in response to viral infection and inflammation. Further, it has been shown that pre-
351 existing neutralizing anti-type I interferon antibodies, which can be found in about 10% of
352 patients with severe COVID-19 pneumonia, are related to the highest risk of developing life-
353 threatening COVID-19 disease[50]. Therefore, the *de novo* induction of anti-cytokine auto-
354 antibodies in a large proportion of hospitalized COVID-19 patients as described by Chang et
355 al[49], might indeed represent the origin of circulating sICs in COVID-19. In such a scenario,
356 immune responses are deviated first by depletion of important cytokines and second through
357 the formation of pathological sICs which trigger immunological damage. We show that
358 critically diseased patients show significantly higher levels of reactive sICs compared to less
359 severely diseased patients. In addition, sIC responses can be found significantly earlier in
360 critically diseased patients, which was associated with a fatal disease outcome. We also find
361 that patients show a wide range of sIC reactivity. According to the Heidelberger-Kendall
362 precipitation curve[51], sIC size is critically dependent on the antigen:antibody stoichiometry. As

363 the used FcγR activation assay is sensitive to sIC size[17], it is highly likely that this also plays a
364 role when measuring COVID-19 patient serum. As some patients show high anti-SARS-CoV-
365 2-S IgG titers in the absence of sICs and vice versa we speculate that sIC size plays a role in
366 CD16 reactivity. Therefore, we propose that in addition to the presence of sICs, the size of sICs
367 plays a role in CD16 driven COVID-19 immunopathology.
368 Taken together, we conclude that CD16 activation in COVID-19 disease is governed by IgG
369 glycan profiles and sIC formation (Figure 5) and plays a major role in disease progression and
370 severity. Indeed, there is evidence in this direction from a clinical perspective provided by a
371 recent study that finds the administration of intravenous immunoglobulin (IVIg) to alleviate
372 COVID-19 disease[52]. Although no direct proof, this heavily implies that the saturation of FcγRs
373 mitigates immunopathology. Therefore, our findings provide an explanation for the sustained
374 immunopathology following SARS-CoV-2 infection as well as for the efficacy of IVIg
375 treatment in severe to critical COVID-19 disease.
376
377
378 **Material and Methods**
379
380 **Subjects and specimens**
381 Between March 2020 and April 2020, 41 patients with SARS-CoV-2 infection confirmed by
382 real-time PCR were hospitalized in the University Medical Center, Freiburg. Serum samples
383 were collected during hospitalization for routine laboratory testing. Clinical data were obtained
384 from electronic medical records. A total of 27 patients necessitating invasive mechanical
385 ventilation were included in the critical group. Fourteen patients requiring O_2 supplementation
386 were included in the severe group. Additionally, serum samples from 29 mild COVID-19 cases
387 and 30 healthy donor (HD) plasma samples were used as controls in this study.
388
389 **Cell culture**
390 African green monkey kidney Vero E6 cells (ATCC CRL-1586) were cultured at 37°C in
391 Dulbecco's Modified Eagle Medium (DMEM) supplemented with 10% (vol/vol) fetal calf
392 serum (FCS, Biochrom), sodium pyruvate (1x, Gibco) and 100 U/ml penicillin-Streptomycin
393 (Gibco). BW5147 mouse thymoma cells (BW, obtained from ATCC: TIB-47) were stably
394 transduced with human FcγR as previously described[53]. Cells were maintained at $3x10^5$ to $9x10^5$
395 cells/ml in Roswell Park Memorial Institute medium (RPMI GlutaMAX, Gibco) supplemented
396 with 10% (vol/vol) FCS, sodium pyruvate (1x, Gibco), 100 U/ml penicillin-Streptomycin

397 (Gibco) β-mercaptoethanol (0.1 mM, Gibco). Cells were cultured at 37°C, 5% CO_2. All cell
398 lines were routinely tested for mycoplasma.
399
400 **Monitoring of antibody response to SARS-CoV-2 by ELISA**
401 Serum IgG antibody titers targeting S1- and N-SARS-CoV-2 proteins were measured using
402 commercial enzyme-linked immunosorbent assay (ELISA). Anti-S1- SARS-CoV-2 IgG was
403 measured by the anti-SARS-CoV-2 ELISA (IgG) Euroimmune Kit (Euroimmune, Lübeck,
404 Germany) according to manufacturer's protocol. Results were evaluated semi-quantitatively by
405 calculation of a ratio of the extinction of the control or patient sample over the extinction of the
406 calibrator. This ratio is interpreted as follows: < 0.8 negative; ≥ 0.8 to <1.0 borderline; ≥ 1.1
407 positive. Anti-N SARS-CoV-2 IgG was detected using the recomWell SARS-CoV-2 IgG Kit
408 (Mikrogen Diagnostik GmbH, Neuried, Germany) according to manufacturer's protocol. The
409 corresponding antibody activity in units per ml is allocated to the absorbance values. Result
410 values are interpreted as follow: U/ml < 20 negative; 20 <U/ml > 24 borderline; U/sample > 24
411 positive. IgG against the SARS-CoV-2 Spike Glycoprotein Receptor Binding Domain (RBD)
412 were detected using SARS-CoV-2 IgG ELISA Reagent Set, kindly provided from InVivo
413 (InVivo Biotech Services GmbH, Hennigsdorf, Germany) according to manufacturer's
414 protocol.
415
416 **Fcγ receptor activation assay**
417 FcγRIIIA (CD16A, 158V) activation was measured by a cell-based assay as previously
418 described[28]. For detection of anti-S and anti-RBD-specific FcγR activation we utilized SARS-
419 CoV-2-S- and RBD-coated plates (kindly provided by InVivo Biotech Services GmbH,
420 Hennigsdorf, Germany). The recombinant (S)-protein was produced under serum-free
421 conditions in mammalian cells and contains amino acid residues 1 to 1213 of the SARS-CoV-
422 2 Wuhan-Hu-1-isolate (GenBank annotation QHD43416.1). The furin cleavage site was
423 mutated, two mutations for protein stabilization were included, and the C-terminal domain was
424 replaced by a T4 trimerization sequence and a C-terminal hexa-His-Tag[54] The recombinant
425 RBD-protein represented amino acids 319 to 541 of the (S)-protein mentioned before. Both
426 recombinant proteins were purified using immobilized metal exchange chromatography
427 (IMAC) and preparative SEC under standard conditions in a regulated environment. Microtiter
428 plates were coated using 0.2 µg recombinant (S)-protein or RBD-protein per well. N-specific
429 FcγR activation was determined using plates coated with SARS-CoV-2-N (Mikrogen
430 Diagnostik GmbH, Neuried, Germany). Respective plates were subsequently incubated with

431 serial dilutions of SARS-CoV-2 positive sera or control sera in RPMI supplemented with 10%
432 (vol/vol) FCS for 30 min at 37°C. All wells were thoroughly washed before co-cultivation with
433 BW5147 reporter cells for 16 h at 37°C, 5% CO_2. Cross-link activation of reporter cells was
434 performed by direct coating of target antibody to ELISA plate (Nunc Maxisorp; 96 well, flat
435 transparent), followed by a blocking step and incubation with 2×10^5 reporter cells per well.
436 For all activation assays, mouse IL-2 secretion was quantified by anti-IL-2 ELISA, as described
437 earlier. FcγRIIIA (CD16A) activation by sICs was measured by a recently developed cell-based
438 assay[17]. Briefly, $2x10^5$ BW5147-CD16 reporter cells were incubated with SARS-CoV-2 sera in
439 a total volume of 200 µl for 16 h at 37°C, 5% CO_2. Incubation was performed in a 96-well
440 ELISA plate (Nunc Maxisorp) pre-treated with PBS containing10% FCS for 1 h at 4°C to avoid
441 direct binding of serum IgG to the plate. Reporter cell mIL-2 secretion was quantified via
442 ELISA as described previously[28].
443
444 **Purification of SARS-CoV2-S and –N specific antibodies from serum**
445 SARS-CoV-2-specific antibodies were purified using SARS-CoV-2 spike protein (S)-coated
446 plates (kindly provided by InVivo BioTech Services) and - nucleocapsid (N) - coated plates
447 recomWell SARS-CoV-2 IgG (Mikrogen Diagnostik GmbH, Neuried, Germany). Patient sera
448 were diluted 1:5 in 100 µl (two wells per serum sample) and incubated for one hour at 37°C
449 with the S- and N-precoated plates. After washing using PBS-T (0.05% Tween 20) 100 mM
450 formic acid (30 µl/well) was added and incubated for 5 min on an orbital shaker at room
451 temperature (RT) to elute bound IgG. Following pH neutralization using TRIS buffer (1 M),
452 the eluates were either directly processed or stored at 4°C.
453
454 **Quantitation of antigen-specific IgG amount**
455 In order to determine the relative S1- and N-SARS-CoV-2 specific IgG antibody concentration
456 of the generated eluates, S1- and N-ELISA were performed by the anti-SARS-CoV-2 ELISA
457 (IgG) Euroimmune Kit (Euroimmune, Lübeck, Germany) and anti-N SARS-CoV-2 IgG ELISA
458 (recomWell SARS-CoV-2 IgG Kit (Mikrogen Diagnostik GmbH, Neuried, Germany) as
459 aformentioned.
460
461 **Analysis of antigen-specific IgG-Fcγ fucosylation**
462 Fucosylation levels of S- and N-specific IgG were measured using a lectin-based ELISA assay.
463 Briefly, 96-well Maxisorb plates (Nunc®) were coated with 50µl/well anti-human IgG-Fab
464 fragment (MyBiosource, MBS674607) at a concentration of 2 µg/ml, diluted in PBS for one

465 hour at 37°C. After three washing steps with PBS-T (0.05% Tween20) unspecific binding sites
466 were blocked adding 300 µl/well Carbo-free™ blocking solution (VectorLab, Inc., SP-5040,
467 LOT: ZF0415) for one hour at room temperature. After three further washing steps, eluted
468 antibodies were 2-fold serially diluted with PBS in a total volume of 30 µl/well and incubated
469 for one hour at 37°C and 5% CO_2. After washing (3x) using PBS-T, 50 µl/well of 4 µg/ml
470 biotinylated Aleuria Aurantia lectin (AAL, lectin, VectorLab, B-1395) diluted in lectin buffer
471 (10 mM HEPES, 0.1 mM $CaCl_2$, 0.15 M NaCl, 0.1% Tween20) was added and incubated for
472 45 min at room temperature (RT). Following another three washing steps using PBS-T,
473 Streptavidin-Peroxidase Polymer (Sigma, S 2438), at 1 µg/ml final concentration diluted in
474 LowCross-HRP®-buffer (Candor, Order #.: 200 500) was added and incubated for one hour at
475 RT. After washing five times with PBS-T, 50 µl/well of 1-Step™ Ultra TMB-ELISA Substrate
476 Solution (ThermoFisher, 34028) was applied and the enzyme-substrate reaction was stopped
477 after six minutes using 50 µl/well sulphuric acid (1 M H_2SO_4). Quantification of absorbance,
478 OD_{450nm}, was performed using a Tecan M2000.
479
480 **PEG Precipitation**
481 Sera pools, consisting of eight different sera per pool, were diluted with varying amounts of
482 PEG8000, in order to reach a final PEG8000 concentration of 1, 2, 3.5, 5 and 7.5% respectively.
483 Mixtures were vortexed and incubated overnight at 4°C. For supernatant analysis, precipitates
484 were sedimented via centrifugation at 13.000 rpm for 30 minutes at 4°C. For Mass Spectrometry
485 analysis, PEG8000-precipitated sICs were shortly run into 10% polyacrylamide gels. After
486 over-night fixation (40% ethanol, 10% acetic acid, 50% water) and washing (3x), complete
487 lanes were excised.
488
489 **Benzonase treatment of sera**
490 Serum from six individual patients containing CD16-reactive soluble immune complexes, were
491 treated with 250 units (U) of Benzonase Nuclease (Sigma-Aldrich Chemie Gmbh, Munich
492 Germany) for 1 h at 4°C. After treatment, sera were titrated in complete BW5147 culture
493 medium and tested for CD16 reactivity. Non-treated sera served as control. To verify
494 Benzonase activity in the presence of human serum, 3 µg of pIRES-eGFP plasmid DNA
495 (Addgene) were digested with 250 U of Benzonase. Successful nucleic acid digestion was
496 visualized using a 1% agarose gel stained with Midori Green.
497
498 **Immune precipitation**

499 For mass spectrometry analysis of SARS-CoV2-S specific precipitates, individual sera
500 containing CD16-reactive soluble immune complexes were subjected to immune precipitation
501 (IP) using Pierce MS-compatible magnetic IP kit (ThermoFisher Scientific, Darmstadt,
502 Germany) according to manufacturer's protocol. Briefly 250 µl serum was incubated overnight
503 at 4°C with 5 µg of biotinylated anti-RBD-specific TRES-1-224.2.19 mouse monoclonal
504 antibody or TRES-II-480 (isotype control) (kind gift of H.M. Jäck, Erlangen) before addition
505 of streptavidin magnetic beads. Beads were subsequently collected via centrifugation and
506 elution buffer was added to detach putative precipitated antigen. The elution was dried in a
507 speed vacuum concentrator and shortly run into 10% polyacrylamide gels. After over-night
508 fixation (40% ethanol, 10% acetic acid, 50% water) and washing (3x), complete lanes were
509 excised. Antibody biotinylation was performed using a Pierce antibody biotinylation Kit for IP
510 (ThermoFisher Scientific, Darmstadt, Germany) according to manufacturer's protocol.
511
512 **Mass Spectrometry**
513 Proteins were in-gel digested with sequencing grade modified trypsin (Promega GmbH,
514 Walldorf, Germany) similar to the procedure described by Pandey et al.[55]. Vacuum-dried
515 peptides were dissolved in 0.5% trifluoroacetic acid, loaded onto a trap column (C18
516 PepMap100, 5 µm particles, Thermo Fisher Scientific GmbH, Dreieich, Germany) with 0.05%
517 trifluoroacetic acid (4 min, 10 µL/min) and separated on a C18 reversed phase column
518 (SilicaTip™ emitter, 75 µm i.d., 8 µm tip, New Objective, Inc, Littleton, USA, manually packed
519 23 cm with ReproSil-Pur ODS-3, 3 µm particles, Dr. A. Maisch HPLC GmbH, Ammerbuch-
520 Entringen, Germany; flow rate: 300 nL/min). For sample injection and multi-step gradient
521 formation (eluent "A": 0.5% acetic acid in water; eluent "B": 0.5% acetic acid in 80%
522 acetonitrile / 20% water; gradient length / acquisition time: 100 min or 175 min) an UltiMate
523 3000 RSLCnano system (Thermo Fisher Scientific GmbH, Dreieich, Germany) was used.
524 Eluting peptides were electrosprayed at 2.3 kV via a Nanospray Flex ion source into a Q
525 Exactive HF-X hybrid quadrupole-orbitrap mass spectrometer (both Thermo Fisher Scientific
526 GmbH, Dreieich, Germany) and analyzed by data-dependent acquisition with HCD (higher
527 energy collisional dissociation) fragmentation of doubly, triply and quadruply charged ions
528 (loop count and dynamic exclusion dependent on the gradient length). Peak lists were generated
529 with ProteoWizard msConvert (http://proteowizard.sourceforge.net/; version 3.0.11098), linear
530 shift mass recalibrated (after a preliminary database search) using in-house
531 developed software and searched against a database containing the SARS-CoV-2 UniProtKB
532 reference proteome (proteome ID: UP000464024), all human UniProtKB/Swiss-Prot entries,

533 and optionally (to reduce the number of incorrectly assigned matches) selected bacterial
534 proteins (finally the Pseudomonas fluorescens (strain SBW25) reference proteome;
535 proteome ID: UP000002332) with Mascot 2.6.2 (Matrix Science Ltd, London, UK; peptide
536 mass tolerance: ± 5 ppm; fragment mass tolerance: ± 20 mmu; one missed trypsin cleavage and
537 common variable modifications allowed).
538
539 **Neutralization assay**
540 Serum neutralization capacity was analyzed as previously described[56]. Briefly, VeroE6 cells
541 were seeded in 12-well plates at a density of $2.8x10^5$ cells/well 24 h prior to infection. Serum
542 samples were diluted at ratios of 1:16, 1:32 and 1:64 in 50 µL PBS total volume. Negative
543 controls (PBS without serum) were included for each serum. Diluted sera and negative controls
544 were subsequently mixed with 90 plaque forming units (PFU) of authentic SARS-CoV-2 (B.1)
545 in 50 µl PBS (1600 PFU/mL) resulting in final sera dilution ratios of 1:32, 1:64, and 1:128.
546 Following incubation at RT for 1 h, 400 µL PBS was added to each sample and the mixture
547 was subsequently used to infect VeroE6 cells. After 1.5 h of incubation at RT, inoculum was
548 removed and the cells were overlaid with 0.6% Oxoid-agar in DMEM, 20 mM HEPES (pH
549 7.4), 0.1% $NaHCO_3$, 1% BSA and 0.01% DEAE-Dextran. Cells were fixed 48h post-infection
550 (4% formaldehyde for 30 minutes). Upon removal of the agar overlay, plaque neutralization
551 was visualized using 1% crystal violet. PFU were counted manually. Plaques counted for
552 serum-treated wells were compared to the average number of plaques in the untreated negative
553 controls, which were set to 100%.
554
555 **Statistical analyses**
556 Statistical analyses were performed using linear statistical models. i.e. the two-group
557 comparisons were made based on the t-statistic of the estimated effects. Differences over more
558 than two groups were tested by Analysis of Variance (ANOVA) and multiple testing for
559 subsequent two-group comparisons was then considered by performing Games-Howell post-
560 hoc tests. For the time course data, patient differences were treated as random effects in a linear
561 mixed effects model with time and clinical course (severe vs. critical) as fixed main and
562 interaction effects. All analyses were performed at the log_2 scale. Assumptions about variance
563 heterogeneity and normal distribution were checked by visual inspection of diagnostic plots.
564
565 **Ethics**

The protocol of this study conforms to the ethical guidelines of the 1975 Declaration of Helsinki and was approved by the institutional ethical committee of the University of Freiburg (EK 153/20). Written informed consent was obtained from participants and the study was conducted according to federal guidelines, local ethics committee regulations (Albert-Ludwigs-Universität, Freiburg, Germany: No. F-2020-09-03-160428 and no. 322/20)

572 **Figure Legends**

573

574 **Figure 1**

575 **IgG responses against different SARS-CoV-2 proteins across severe and critical clinical**
576 **course of disease.**

577 IgG antibody levels were analyzed in longitudinal serum samples from hospitalized SARS-
578 CoV-2 infected individuals. 27 patients were categorized as critically diseased when in need of
579 invasive mechanical ventilation (red symbols) compared to 14 severely diseased patients who
580 did not require invasive ventilation (blue symbols). (A) IgG response against SARS-CoV-2 S1
581 –protein and (B) SARS-CoV-2 N-protein as determined by commercial ELISA assays. Dotted
582 lines represent cut-off values for commercial S1- and N- specific ELISA assays. Each dot
583 represents the mean value obtained by the analysis of all samples which were available at the
584 indicated time points following symptom onset. Solid black lines indicate the median. (C)
585 Serum neutralization capacity against SARS-CoV-2 measured by a plaque reduction assay. Sera
586 were considered neutralizing upon 50% plaque reduction (dotted line) at a 1:64 dilution. Solid
587 black lines indicate the median. Significant differences were tested using a linear mixed effects
588 model (***, $p<0.001$; *, $p<0.05$).

589

590 **Figure 1-figure supplement 1**

591 **SARS-CoV-2 specific IgG levels in seronegative patients and according to disease**
592 **outcome.**

593 A) S1- and B) N-specific IgG levels in 30 healthy donors. Solid black lines indicate the median.
594 C) Cumulative S1-, D) N- and E) RBD-specific IgG levels measured 13-25 days after symptom
595 onset in deceased (black symbols) and not deceased COVID-19 patients (blue symbols). Solid
596 black lines indicate the median.

597

598 **Figure 1-figure supplement 2**

599 **Longitudinal changes in anti- SARS-CoV-2 IgG titers in severely and critically diseased**
600 **patients.**

601 Serial serum samples were collected from hospitalized COVID-19 patients and used for SARS-
602 CoV-2–specific IgG measurement. IgG responses against SARS-CoV-2 S1- and N-protein in
603 (A, C) critically (red symbols) and (B, D) severely (blue symbols) diseased patients. Dotted
604 lines represent cut-off values for commercial S1- and N- specific ELISA assays. Each symbol
605 represents the mean value of all samples which were available for each patient at the indicated

606 time range after symptom onset. There are no significant t-tests (i.e. $p>0.05$ for all
607 comparisons).
608
609 **Figure 2**
610 **CD16 activation by SARS-CoV-2 - specific IgG is enhanced in critically diseased patients**.
611 FcγRIII activation by SARS-CoV-2-specific IgG on BW5147 reporter cells in serum samples
612 obtained 13-25 days following symptom onset from 23 critically (red symbols) and 14 severely
613 (blue symbols) diseased patients. Between 2 to 8 samples/patient were analyzed depending on
614 the availability of sample material. Sera from 29 non-hospitalized patients with mild SARS-
615 CoV-2 infection (grey symbols) and 30 healthy donors (open circles) served as reference. Each
616 symbol represents the mean value of all available samples per patient. (A, B, C) ELISA levels
617 for S1- N- and RBD-specific IgG. Dotted lines represent cut-off values for commercial S1-, N-
618 and RBD - specific ELISA assays. Solid black lines indicate the mean. (D, E, F) FcγRIII
619 activation by S-, N- and RBD-specific IgG expressed as $\log_2$ fold change relative to negative
620 control. Solid black lines indicate the mean. (G, H, I) FcγRIII activation, expressed as $\log_2$
621 values relative to SARS-CoV-2-spcific IgG titers. Solid black lines indicate the mean.
622 Significant differences over all three groups were tested by ANOVA and pairwise group
623 comparison was made by Games-Howell post-hoc tests (***, $p<0.001$; **, $p<0.01$; *, $p<0.05$).
624
625 **Figure 2-figure supplement 1**
626 **Cell-based reporter assay measuring CD16 activation in response to immobilized IgG and**
627 **sICs**. BW5147 reporter cells expressing chimeric human FcγRIII secrete IL-2 in response to
628 FcγR activation by A) clustered viral specific IgG binding solid-phase antigen or B) soluble
629 ICs. Solubility of sICs is achieved by pre-blocking an ELISA plate with PBS supplemented
630 with 10% FCS as previously described[17].
631
632 **Figure 2-figure supplement 2**
633 **Dose dependent CD16 activation by SARS-CoV-2 specific IgG.**
634 CD16 activation by A) S- , B) N- and C) RBD-specific IgG in 9 representatively selected serum
635 samples and one SARS-CoV-2 negative serum (dark blue bars). Sera were serially diluted at
636 1:20, 1:100, 1:500 and 1:2500. FcγRIII activation initiates IL-2 secretion by reporter cells,
637 which is subsequently measured via ELISA (OD 450 nm). Based on this empirical pretesting
638 all sera were thereafter tested at 1:100 and 1:500 dilutions to reach an optimal dynamic range

639 of response. The OD values obtained by the 1:500 dilutions were used for subsequent data
640 analysis.
641
642 **Figure 2-figure supplement 3**
643 **Reproducibility of CD16 activation measurements by SARS-CoV-2 specific IgG.** Selected
644 sera which were available in sufficient amount from patients with critical (red symbols) or
645 severe (blue symbols) SARS-CoV-2 infection were tested in two independent experiments to
646 show reproducibility and consistency of results. CD16 activation by S-, N- and RBD specific
647 IgG is shown. Statistical tests using a Kolmogorov-Smirnov test indicate no significant
648 differences.
649
650 **Figure 2-figure supplement 4**
651 **Correlation of CD16 activation by virus specific IgG and ELISA levels.**
652 Pearson's correlation coefficient was used to assess the relationship between virus–specific IgG
653 levels and their capability to trigger CD16 activation on BW5147 reporter cells in 22 paired
654 samples from patients with critical disease (red symbols), 14 paired samples from patients with
655 severe disease (blue symbols) and 28 samples from patients with mild disease (grey symbols).
656 Each dot represents the mean value obtained by the analysis of all samples available at the
657 indicated time points. (A-C) anti-S IgG, (D-F) anti-N IgG and anti-RBD-IgG (E-I).
658
659 **Figure 3**
660 **Anti SARS-CoV-2 IgG Fc core fucosylation in critical and severe COVID-19 cases.**
661 IgG-Fc core fucosylation levels of SARS-CoV-2 –specific IgG in critically (red bars) and
662 severely (blue bars) diseased COVID-19 patients. Analysis was carried out on a pool of 5
663 different sera. Measured OD values for fucosylation of the generated eluates were normalized
664 to their respective IgG titers determined by antigen-specific S1 and N ELISA. A) S-IgG-Fc-
665 fucosylation and B) N-IgG-Fc-fucosylation in critically and severely diseased patients
666 characterized by either high (red) or low (patterned) CD16-activation levels in the FcγR
667 activation reporter assay. The mean and standard deviation (SD) of at least three independent
668 experiments is depicted. Statistical tests using a two-factorial linear model indicate three
669 significant differences between the low and high categories (***, $p<0.001$; **, $p<0.01$; *,
670 $p<0.05$; ns = not significant).
671 **Figure 4**
672 **Severe COVID-19 disease coincides with high CD16 activation by sICs.**

673 Serial serum samples obtained 13-25 days after onset of symptoms were analyzed in a cell-
674 based reporter assay which is sensitive to sIC amount and size[16]. FcγR activation is shown as
675 log_2 fold change relative to negative control. Each symbol represents the mean value obtained
676 by the analysis of all samples available in the indicated time range for each individual patient.
677 A) Analysis of CD16 activation by sICs in SARS-CoV-2-infected patients compared to healthy
678 blood donors B) Levels of IC-mediated CD16 activation across severe, critical and mild clinical
679 courses of COVID-19 disease, in healthy donors (HD) and in non-COVID-19- patients who
680 developed acute respiratory distress syndrome (ARDS). Solid black lines indicate the mean.
681 Two-group comparisons with the linear model indicate significant differences between critical
682 cases and all other groups, as well as between severe cases and all other groups (***, $p<0.001$;
683 **, $p<0.01$). No significant differences ($p>0.05$) have been found for the comparisons mild vs.
684 healthy and for HD vs. ARDS. C) Kinetics of IC-mediated CD16 activation in critically and
685 severely diseased patients. Solid black lines indicate the median. The mixed effects model
686 indicates two time points with significant differences (**, $p<0.01$; *, $p<0.05$).
687
688 **Figure 4-figure supplement 1**
689 **CD16 activation by sICs in non-COVID-19 patients with ARDS.**
690 Serum samples from 47 patients with ARDS in response to infections of different etiology were
691 analyzed in a cell-based reporter assay which is sensitive to sIC amount and size[16]. FcγR
692 activation is shown as log_2 fold change relative to negative control. Each symbol represents one
693 sample from one patient. CMV: Cytomegalovirus reactivation under immunosuppression; HIV:
694 HIV infection; TBC: Mycobacterium tuberculosis infection; Influenza: influenza virus
695 infection; TX: solid organ transplantation. Solid black lines indicate the median.
696
697 **Figure 4-figure supplement 2**
698 **PEG precipitation eliminates sIC-mediated CD16 activation.**
699 Pools of 8 sera were incubated with equal volumes of PEG8000 to reach the indicated final
700 PEG concentrations. A) CD16 activation after PEG-precipitation in the pool supernatant,
701 showing either high (sICs+) or no (sICs-) CD16 activation. Sera from healthy donors (HD)
702 were included as a negative control. Activation levels are expressed as IL-2 levels (OD 450 nm)
703 released by reporter cells. The mean and SD of two independent experiments is depicted. B)
704 Anti SARS-CoV-2 IgG levels against S1 (left panel) or N (right panel) IgG following PEG
705 precipitation. The mean and SD of two independent experiments (sIC+/sIC-) is depicted.
706

707 **Figure 4-figure supplement 3**

708 **Individual CD16 activation by sICs and anti-S1 ELISA IgG kinetics post symptoms onset.**

709 Individual sera for either critically or severely diseased patients were analyzed in order to detect
710 anti S1-IgG antibodies (top panel) via Euroimmune ELISA [AU] and CD16 activation by
711 soluble immune complexes (lower panel, relative CD16 activation depicted as fold increase to
712 the negative control) over time (1-40 days post symptom onset). White panel: not tested.

713

714 **Figure 4-figure supplement 4**

715 **Benzonase treatment of sIC-reactive sera does not abolish CD16 activation.**

716 Left panel: sIC-mediated CD16 reactivity expressed as $\log_2$ fold increase to the negative
717 control, in serum of six individual patients before and after treatment with 250 Units of
718 Benzonase Nuclease. Right panel: As positive control, 3 µg plasmid DNA was digested. M:
719 1kb DNA ladder, Lane 1: benzonase digestion in the presence of human serum, lane 2: plasmid
720 DNA w/o benzonase in the presence of human serum, lane 3: benzonase digestion in medium
721 only and lane 4: plasmid DNA w/o benzonase in medium only.

722

723

724 **Figure 5**

725 **Summary of antibody features from SARS-CoV-2-infected patients with critical and**
726 **severe disease.**

727 Relative multivariate antibody features illustrated as radar chart in critically (red) or severely
728 (blue) diseased COVID-19 patients normalized to the corresponding features of patients with
729 mild infection (grey). Each spoke represents one of the following variables: ELISA (S1-IgG,
730 N-IgG,) and CD16 activation (S-IgG, N-IgG, sICs). Arithmetic mean values of $\log_2$ values were
731 calculated for each group (days 13-25 post symptom onset) respectively. The fold change
732 compared to mildly diseased patients is shown.

733

734

735

736 **Table 1**

737 **Clinical characteristics of the hospitalized SARS-CoV-2 patients.**

738 Patients were categorized as either severely (hospitalized, requiring O_2 supplementation, n=14)
739 or critically diseased (hospitalized and in need of invasive mechanical ventilation, n=27).

740 Diagnostic markers are depicted as mean and SD (in brackets) of all analyzed laboratory
741 parameters obtained 13-25 days post symptom onset. Percentage [%] is indicated.

742 **References**

743

744 1 Zhu, N. *et al.* A Novel Coronavirus from Patients with Pneumonia in China, 2019. *N Engl J Med*
745 **382**, 727-733, doi:10.1056/NEJMoa2001017 (2020).
746 2 Dong, E., Du, H. & Gardner, L. An interactive web-based dashboard to track COVID-19 in real
747 time. *Lancet Infect Dis* **20**, 533-534, doi:10.1016/S1473-3099(20)30120-1 (2020).
748 3 Chen, G. *et al.* Clinical and immunological features of severe and moderate coronavirus disease
749 2019. *J Clin Invest* **130**, 2620-2629, doi:10.1172/JCI137244 (2020).
750 4 Felsenstein, S., Herbert, J. A., McNamara, P. S. & Hedrich, C. M. COVID-19: Immunology and
751 treatment options. *Clin Immunol* **215**, 108448, doi:10.1016/j.clim.2020.108448 (2020).
752 5 Magleby, R. *et al.* Impact of SARS-CoV-2 Viral Load on Risk of Intubation and Mortality Among
753 Hospitalized Patients with Coronavirus Disease 2019. *Clin Infect Dis*, doi:10.1093/cid/ciaa851
754 (2020).
755 6 Ruan, Q., Yang, K., Wang, W., Jiang, L. & Song, J. Correction to: Clinical predictors of mortality
756 due to COVID-19 based on an analysis of data of 150 patients from Wuhan, China. *Intensive*
757 *Care Med* **46**, 1294-1297, doi:10.1007/s00134-020-06028-z (2020).
758 7 Zhou, F. *et al.* Clinical course and risk factors for mortality of adult inpatients with COVID-19 in
759 Wuhan, China: a retrospective cohort study. *Lancet* **395**, 1054-1062, doi:10.1016/S0140-
760 6736(20)30566-3 (2020).
761 8 Yang, X. *et al.* Clinical course and outcomes of critically ill patients with SARS-CoV-2 pneumonia
762 in Wuhan, China: a single-centered, retrospective, observational study. *Lancet Respir Med* **8**,
763 475-481, doi:10.1016/S2213-2600(20)30079-5 (2020).
764 9 Zhou, Y. *et al.* Pathogenic T-cells and inflammatory monocytes incite inflammatory storms in
765 severe COVID-19 patients. *National Science Review* **7**, 998-1002, doi:10.1093/nsr/nwaa041
766 (2020).
767 10 Long, Q. X. *et al.* Antibody responses to SARS-CoV-2 in patients with COVID-19. *Nat Med* **26**,
768 845-848, doi:10.1038/s41591-020-0897-1 (2020).
769 11 Zhang, J. M. & An, J. Cytokines, inflammation, and pain. *Int Anesthesiol Clin* **45**, 27-37,
770 doi:10.1097/AIA.0b013e318034194e (2007).
771 12 Vogelpoel, L. T., Baeten, D. L., de Jong, E. C. & den Dunnen, J. Control of cytokine production
772 by human fc gamma receptors: implications for pathogen defense and autoimmunity. *Front*
773 *Immunol* **6**, 79, doi:10.3389/fimmu.2015.00079 (2015).
774 13 Bruhns, P. & Jonsson, F. Mouse and human FcR effector functions. *Immunol Rev* **268**, 25-51,
775 doi:10.1111/imr.12350 (2015).
776 14 Zubler, R. H. *et al.* Circulating and intra-articular immune complexes in patients with
777 rheumatoid arthritis. Correlation of 125I-Clq binding activity with clinical and biological
778 features of the disease. *J Clin Invest* **57**, 1308-1319, doi:10.1172/JCI108399 (1976).
779 15 Levinsky, R. J. Role of circulating soluble immune complexes in disease. *Arch Dis Child* **53**, 96-
780 99, doi:10.1136/adc.53.2.96 (1978).
781 16 Levinsky, R. J., Cameron, J. S. & Soothill, J. F. Serum immune complexes and disease activity in
782 lupus nephritis. *Lancet* **1**, 564-567, doi:10.1016/s0140-6736(77)91998-5 (1977).
783 17 Chen, H. *et al.* FcγR responses to soluble immune complexes are governed by solubility and
784 size. *bioRxiv*, 2020.2011.2011.378232, doi:10.1101/2020.11.11.378232 (2021).
785 18 Wang, T. T. & Ravetch, J. V. Immune complexes: not just an innocent bystander in chronic viral
786 infection. *Immunity* **42**, 213-215, doi:10.1016/j.immuni.2015.01.022 (2015).
787 19 Carreno, L. J., Pacheco, R., Gutierrez, M. A., Jacobelli, S. & Kalergis, A. M. Disease activity in
788 systemic lupus erythematosus is associated with an altered expression of low-affinity Fc
789 gamma receptors and costimulatory molecules on dendritic cells. *Immunology* **128**, 334-341,
790 doi:10.1111/j.1365-2567.2009.03138.x (2009).
791 20 Faik, I. *et al.* Pyruvate Kinase and Fcgamma Receptor Gene Copy Numbers Associated With
792 Malaria Phenotypes. *J Infect Dis* **216**, 276-282, doi:10.1093/infdis/jix284 (2017).

21 Xu, Z. *et al.* Pathological findings of COVID-19 associated with acute respiratory distress syndrome. *Lancet Respir Med* **8**, 420-422, doi:10.1016/S2213-2600(20)30076-X (2020).
22 Channappanavar, R. & Perlman, S. Pathogenic human coronavirus infections: causes and consequences of cytokine storm and immunopathology. *Seminars in Immunopathology* **39**, 529-539, doi:10.1007/s00281-017-0629-x (2017).
23 Smits, S. L. *et al.* Exacerbated innate host response to SARS-CoV in aged non-human primates. *PLoS Pathog* **6**, e1000756, doi:10.1371/journal.ppat.1000756 (2010).
24 Rockx, B. *et al.* Early upregulation of acute respiratory distress syndrome-associated cytokines promotes lethal disease in an aged-mouse model of severe acute respiratory syndrome coronavirus infection. *J Virol* **83**, 7062-7074, doi:10.1128/JVI.00127-09 (2009).
25 Hoepel, W. *et al.* High titers and low fucosylation of early human anti-SARS-CoV-2 IgG promote inflammation by alveolar macrophages. *Sci Transl Med* **13**, doi:10.1126/scitranslmed.abf8654 (2021).
26 Zohar, T. & Alter, G. Dissecting antibody-mediated protection against SARS-CoV-2. *Nat Rev Immunol* **20**, 392-394, doi:10.1038/s41577-020-0359-5 (2020).
27 Lu, L. L., Suscovich, T. J., Fortune, S. M. & Alter, G. Beyond binding: antibody effector functions in infectious diseases. *Nat Rev Immunol* **18**, 46-61, doi:10.1038/nri.2017.106 (2018).
28 Corrales-Aguilar, E. *et al.* A novel assay for detecting virus-specific antibodies triggering activation of Fe gamma receptors. *J Immunol Methods* **387**, 21-35, doi:10.1016/j.jim.2012.09.006 (2013).
29 Chakraborty, S. *et al.* Proinflammatory IgG Fc structures in patients with severe COVID-19. *Nat Immunol* **22**, 67-73, doi:10.1038/s41590-020-00828-7 (2021).
30 High titers and low fucosylation of early human anti-SARS-CoV-2 IgG promote inflammation by alveolar macrophages. *Sci Transl Med*, doi:10.1126/scitranslmed.abf8654 (2021).
31 Larsen, M. D. *et al.* Afucosylated IgG characterizes enveloped viral responses and correlates with COVID-19 severity. *Science* **371**, doi:10.1126/science.abc8378 (2021).
32 Li, T. *et al.* Modulating IgG effector function by Fc glycan engineering. *Proceedings of the National Academy of Sciences of the United States of America* **114**, 3485-3490, doi:10.1073/pnas.1702173114 (2017).
33 Roncati, L. *et al.* Type 3 hypersensitivity in COVID-19 vasculitis. *Clinical Immunology* **217**, doi:ARTN 108487
10.1016/j.clim.2020.108487 (2020).
34 Roe, K. High COVID-19 virus replication rates, the creation of antigen-antibody immune complexes and indirect haemagglutination resulting in thrombosis. *Transbound Emerg Dis* **67**, 1418-1421, doi:10.1111/tbed.13634 (2020).
35 Zhang, Y. *et al.* Coagulopathy and Antiphospholipid Antibodies in Patients with Covid-19. *N Engl J Med* **382**, e38, doi:10.1056/NEJMc2007575 (2020).
36 Creighton, W. D., Lambert, P. H. & Miescher, P. A. Detection of antibodies and soluble antigen-antibody complexes by precipitation with polyethylene glycol. *J Immunol* **111**, 1219-1227 (1973).
37 Veras, F. P. *et al.* SARS-CoV-2-triggered neutrophil extracellular traps mediate COVID-19 pathology. *J Exp Med* **217**, doi:10.1084/jem.20201129 (2020).
38 Horwitz, J. A. *et al.* Non-neutralizing Antibodies Alter the Course of HIV-1 Infection In Vivo. *Cell* **170**, 637-648 e610, doi:10.1016/j.cell.2017.06.048 (2017).
39 Forthal, D. N. & Moog, C. Fc receptor-mediated antiviral antibodies. *Curr Opin HIV AIDS* **4**, 388-393, doi:10.1097/COH.0b013e32832f0a89 (2009).
40 DiLillo, D. J., Tan, G. S., Palese, P. & Ravetch, J. V. Broadly neutralizing hemagglutinin stalk-specific antibodies require FcgammaR interactions for protection against influenza virus in vivo. *Nat Med* **20**, 143-151, doi:10.1038/nm.3443 (2014).
41 Hessell, A. J. *et al.* Fc receptor but not complement binding is important in antibody protection against HIV. *Nature* **449**, 101-104, doi:10.1038/nature06106 (2007).

42 Li, K. *et al.* Dynamic changes in anti-SARS-CoV-2 antibodies during SARS-CoV-2 infection and recovery from COVID-19. *Nature communications* **11**, 6044, doi:10.1038/s41467-020-19943-y (2020).
43 Ogata, A. F. *et al.* Circulating SARS-CoV-2 Vaccine Antigen Detected in the Plasma of mRNA-1273 Vaccine Recipients. *Clin Infect Dis*, doi:10.1093/cid/ciab465 (2021).
44 Zhang, L. *et al.* SARS-CoV-2 spike-protein D614G mutation increases virion spike density and infectivity. *Nature communications* **11**, 6013, doi:10.1038/s41467-020-19808-4 (2020).
45 Letarov, A. V., Babenko, V. V. & Kulikov, E. E. Free SARS-CoV-2 Spike Protein S1 Particles May Play a Role in the Pathogenesis of COVID-19 Infection. *Biochemistry (Mosc)* **86**, 257-261, doi:10.1134/S0006297921030032 (2021).
46 Woodruff, M. C. *et al.* Extrafollicular B cell responses correlate with neutralizing antibodies and morbidity in COVID-19. *Nat Immunol* **21**, 1506-1516, doi:10.1038/s41590-020-00814-z (2020).
47 Wang, E. Y. *et al.* Diverse functional autoantibodies in patients with COVID-19. *Nature*, doi:10.1038/s41586-021-03631-y (2021).
48 Zuo, Y. *et al.* Prothrombotic autoantibodies in serum from patients hospitalized with COVID-19. *Sci Transl Med* **12**, doi:10.1126/scitranslmed.abd3876 (2020).
49 Chang, S. E. *et al.* New-Onset IgG Autoantibodies in Hospitalized Patients with COVID-19. *medRxiv*, doi:10.1101/2021.01.27.21250559 (2021).
50 Bastard, P. *et al.* Autoantibodies against type I IFNs in patients with life-threatening COVID-19. *Science* **370**, doi:10.1126/science.abd4585 (2020).
51 Heidelberger, M. & Kendall, F. E. A Quantitative Study of the Precipitin Reaction between Type Iii Pneumococcus Polysaccharide and Purified Homologous Antibody. *J Exp Med* **50**, 809-823, doi:10.1084/jem.50.6.809 (1929).
52 Gharebaghi, N., Nejadrahim, R., Mousavi, S. J., Sadat-Ebrahimi, S. R. & Hajizadeh, R. The use of intravenous immunoglobulin gamma for the treatment of severe coronavirus disease 2019: a randomized placebo-controlled double-blind clinical trial. *BMC Infect Dis* **20**, 786, doi:10.1186/s12879-020-05507-4 (2020).
53 Kolb, P. *et al.* Identification and Functional Characterization of a Novel Fc Gamma-Binding Glycoprotein in Rhesus Cytomegalovirus. *J Virol* **93**, doi:10.1128/JVI.02077-18 (2019).
54 Amanat, F. *et al.* A serological assay to detect SARS-CoV-2 seroconversion in humans. *Nat Med* **26**, 1033-1036, doi:10.1038/s41591-020-0913-5 (2020).
55 Pandey, A., Andersen, J. S. & Mann, M. Use of mass spectrometry to study signaling pathways. *Sci STKE* **2000**, pl1, doi:10.1126/stke.2000.37.pl1 (2000).
56 Tönshoff, B. *et al.* Prevalence of SARS-CoV-2 Infection in Children and Their Parents in Southwest Germany. *JAMA Pediatrics* **175**, 586-593, doi:10.1001/jamapediatrics.2021.0001 (2021).

Acknowledgements

We thank Sophia Ruben and Torsten Schulz from InVivo Bio Tech Services for peparing SARS-CoV-2 (S)- and RBD- coated plates and preparing the SARS-CoV-2 IgG ELISA Reagent Set. We thank Hans-Martin Jäck for providing TRES-1-224.2.19 and TRES-II-480 monoclonal antibodies and Quinnlan David for critically reading the manuscript. We also thank Andreas Schlosser for validation of our Mass Spectrometry data. This work was supported by the Bundesministerium fuer Bildung und Forschung (BMBF) through the Deutsches Zentrum fuer Luft- und Raumfahrt, Germany, (DLR, grant number 01KI2077) and by the Federal State of Baden-Wuerttemberg, Germany, MWK-Sonderfoerdermaßnahme COVID-19/AZ.:33-7533.-6-21/7/2 to MS. This work was also supported by an intramural junior investigator fund of the Faculty of Medicine to PK (Hans A. Krebs - Funding for Medical Scientists, Faculty of Medicine, University of Freiburg) and "NaFoUniMedCovid19" (FKZ: 01KX2021 - COVIM to H.H., FKZ 100493916 B-FAST to H.H.) and DFG HE2526/9-1 to H.H.. A. Lother is a member of SFB1425, funded by the Deutsche Forschungsgemeinschaft (DFG, German Research Foundation #422681845). The funders had no role in the study design, data analysis, data interpretation, and in the writing of this report. All authors had full access to the data in the study and accept responsibility to submit for publication.

Author contribution:

Conceived and designed the experiments: J.A., A.M-P., S.G., P.K., A.L, V.F., M.S., H.H.

Performed the experiments: J.A., N.G., U.S., S.G., K. C., W.B.

Analyzed the data: J.A., S.G., P.K., V.F., K.C., A.M-P., W.B., C.K.

Contributed/reagent/sample material: A.B.G., D.H., T.W., N.G.M.

Writing and original draft preparation: J.A., S.G., P.K., V.F.

Review and editing: H.H., M.S., K.C.

Conceptualization: V.F., H.H.

Competing interests: The authors declare the following competing financial interest(s): InVivo BioTech Services is a biotechnology company producing antibodies and proteins, including SARS-CoV-2 antigens.

Data and materials availability: All data associated with this study are present in the paper or Supplementary Materials.

Figures and Tables

Table 1

	All patients n: 41	%	critical n: 27	%	severe n: 14	%
Age [years]	Ø 68 (31-90)	-	Ø 63 (39-79)	-	Ø 76 (31-90)	-
Female	8	19.5	5	18.5	3	21.4
Male	33	80.5	22	81.5	11	78.6
Comorbidities						
Hypertension	21	51.2	12	44.4	9	64.3
Cardiovascular disease	14	34.1	5	18.5	9	64.3
Pulmonary disease	6	14.6	2	7.4	4	28.6
Chronic kidney disease	6	14.6	1	3.7	5	35.7
Diabetes	10	24.4	6	22.2	4	28.6
Malignancy	8	19.5	4	14.8	4	28.6
none	6	14.6	6	22.2	0	0
Diagnostic markers						
Interleukin-6 [pg/ml] Ø	1012.8	-	1452.1 (3774.6)	-	46.1 (26.8)	-
Procalcitonin [ng/ml] Ø	7	-	9.9 (21.9)	-	0.17 (0.11)	-
C- reactive protein [mg/l] Ø	128.1	-	162.2 (75.8)	-	65.3 (47.1)	-
Complications						
Bacterial superinfection	16	39	11	40.7	5	35.7
Treatment						
Hydroxychloroquine, Ritonavir+ Lopinavir (Kaletra®)	24	58.5	18	66.7	6	42.9
Fatal outcome						
Total	11	26.8	10	37	1	7.1

923 **Figure 1**

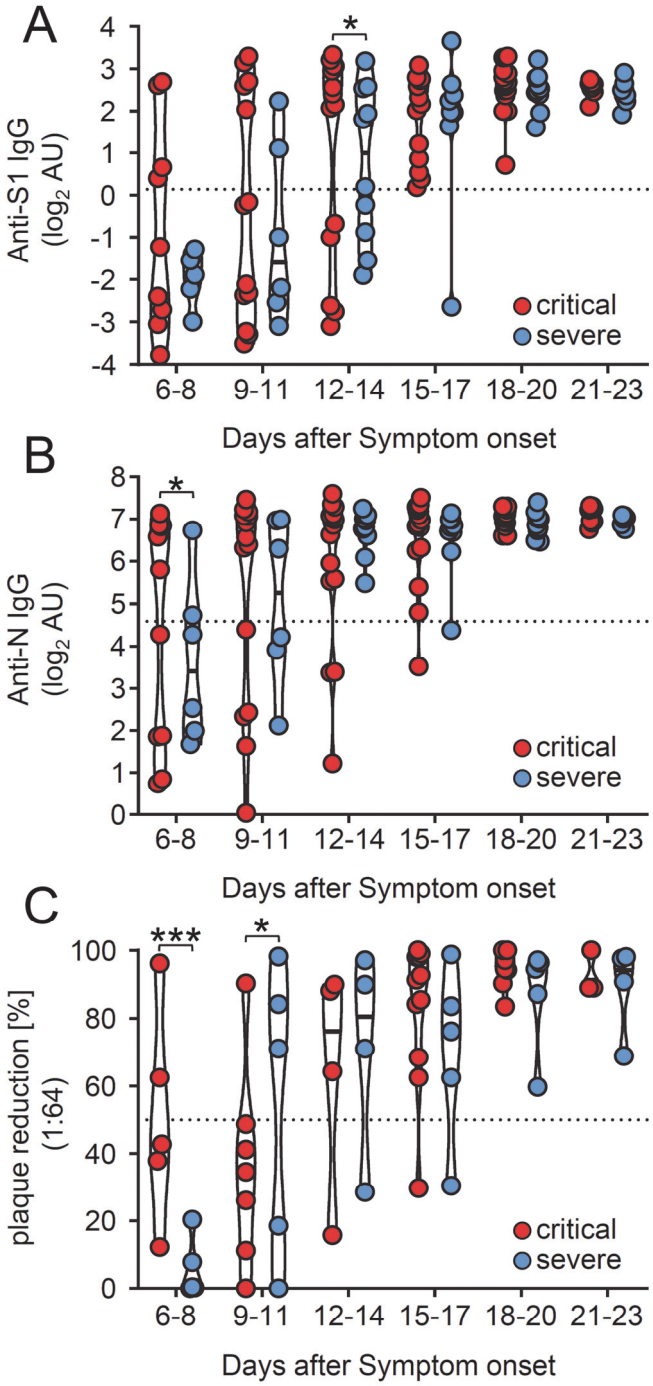

924

925

926

927 **Figure 1 – figure supplement 1**

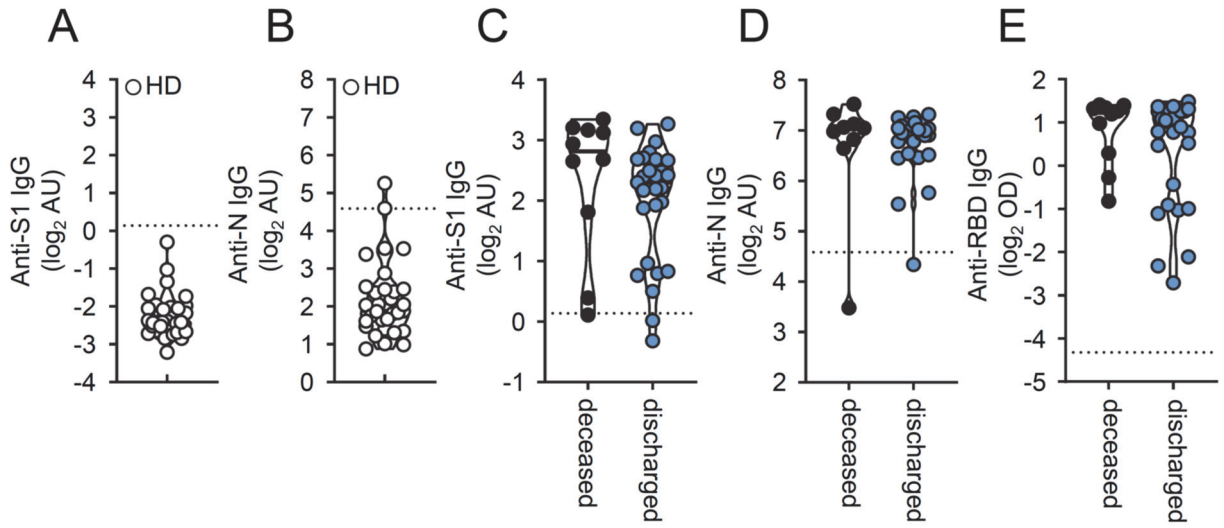

928

929

930 **Figure 1 – figure supplement 2**

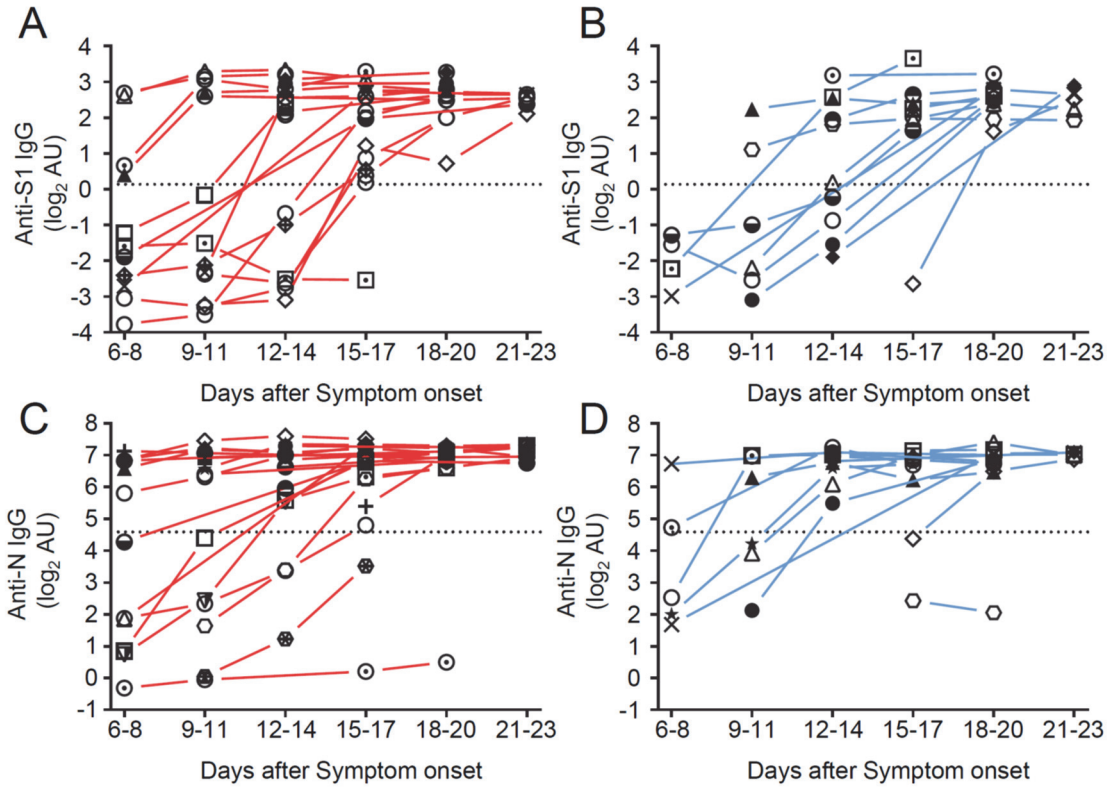

931

932 **Figure 2**

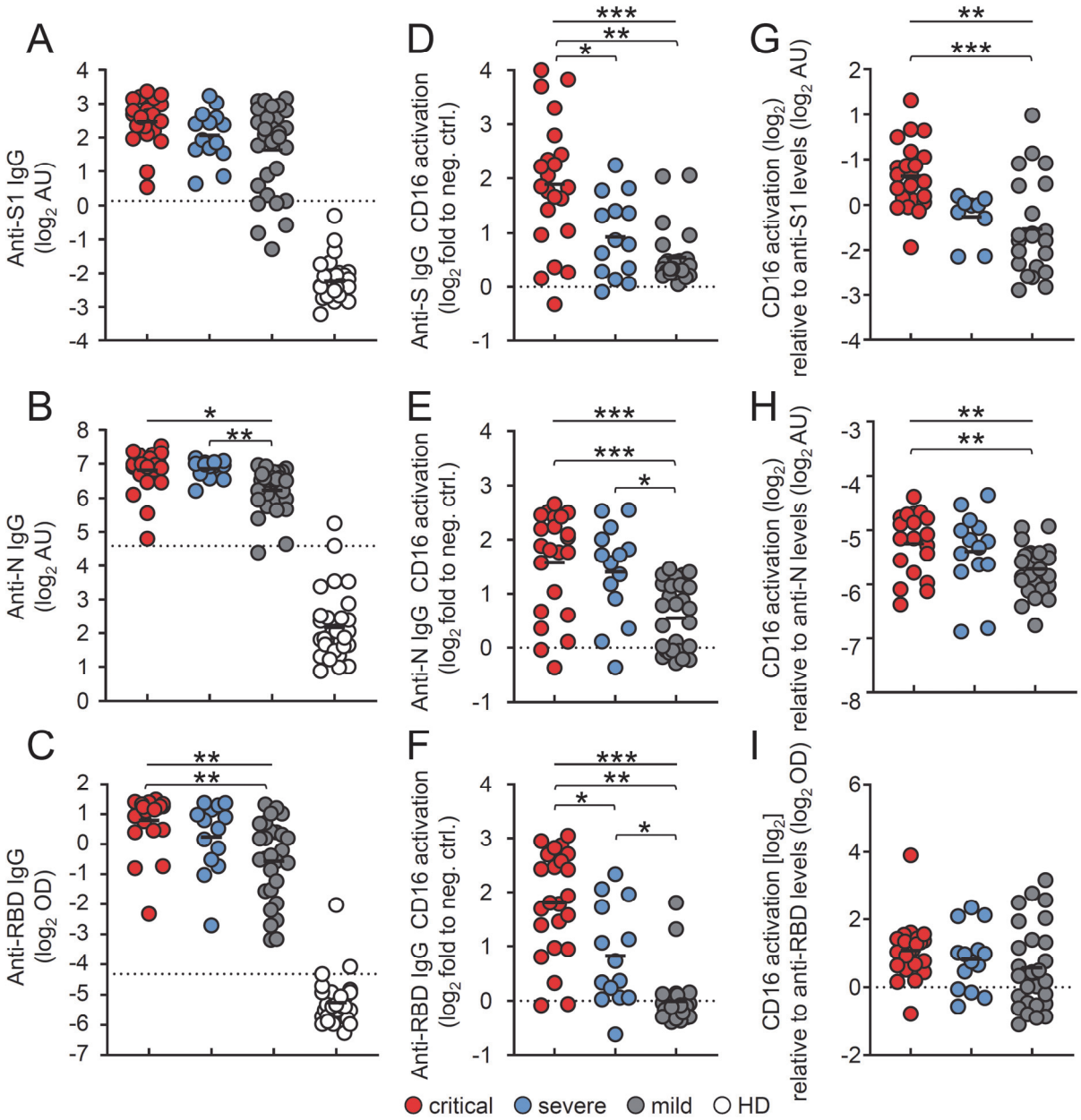

933

934

935 **Figure 2 –figure supplement 1**

936

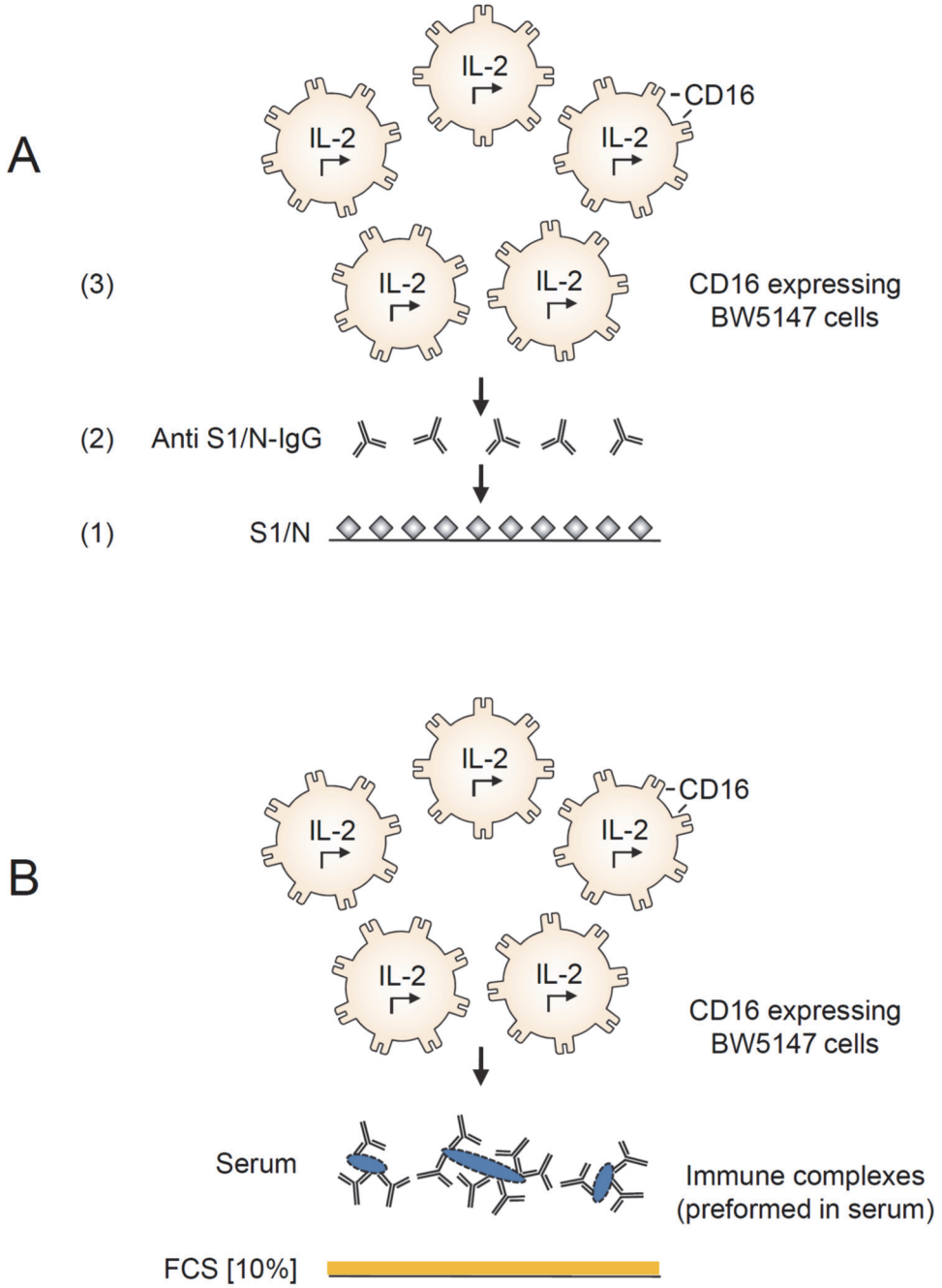

937

938

939 **Figure 2 –figure supplement 2**

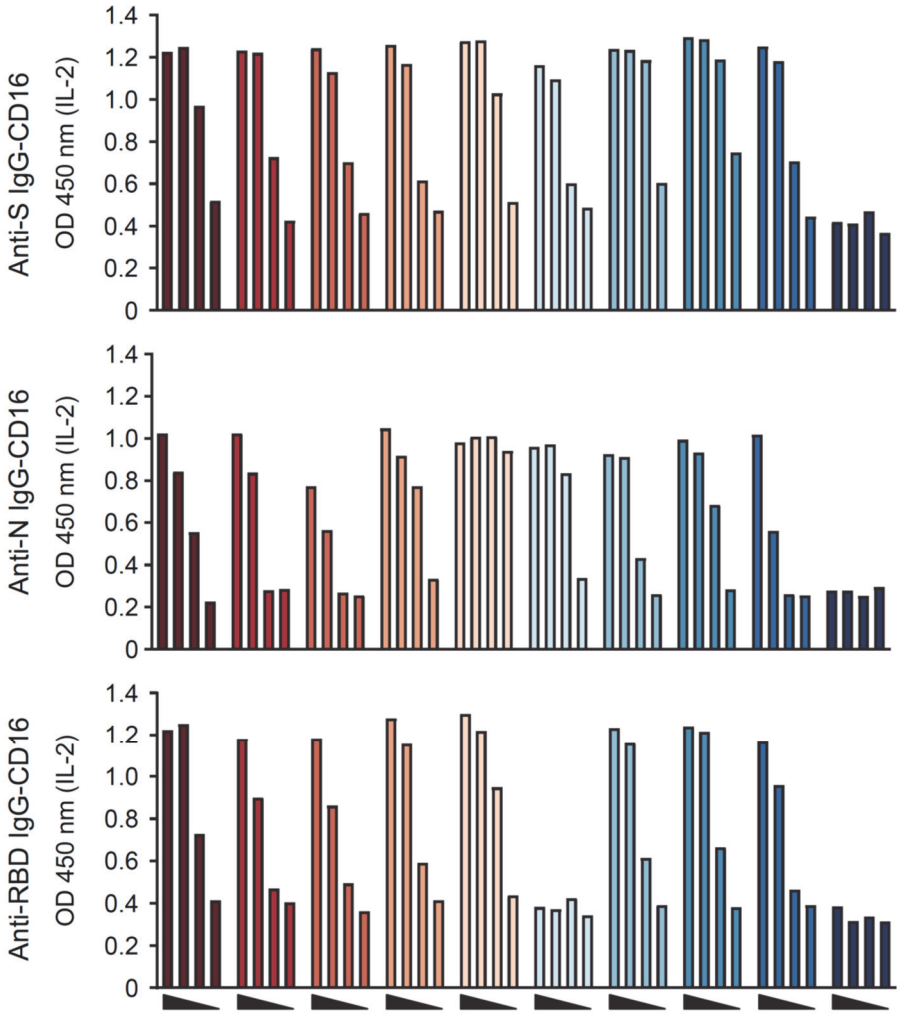

940

941

942 **Figure 2 –figure supplement 3**

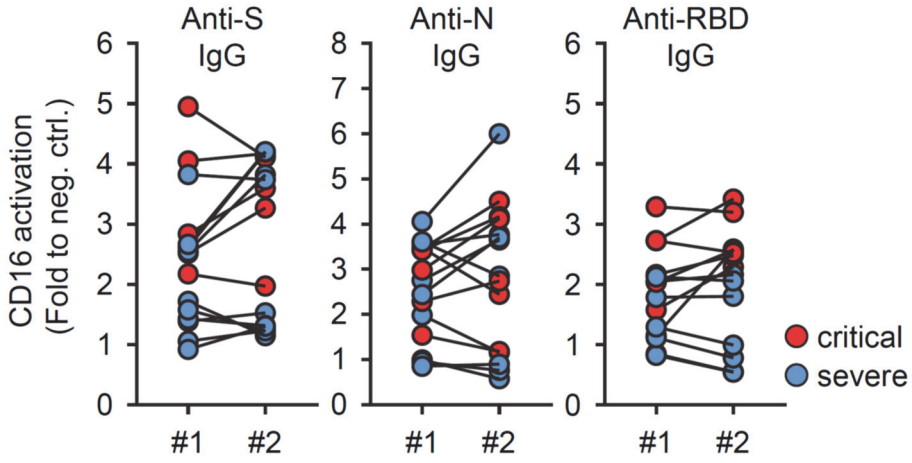

943

944

945 **Figure 2 –figure supplement 4**

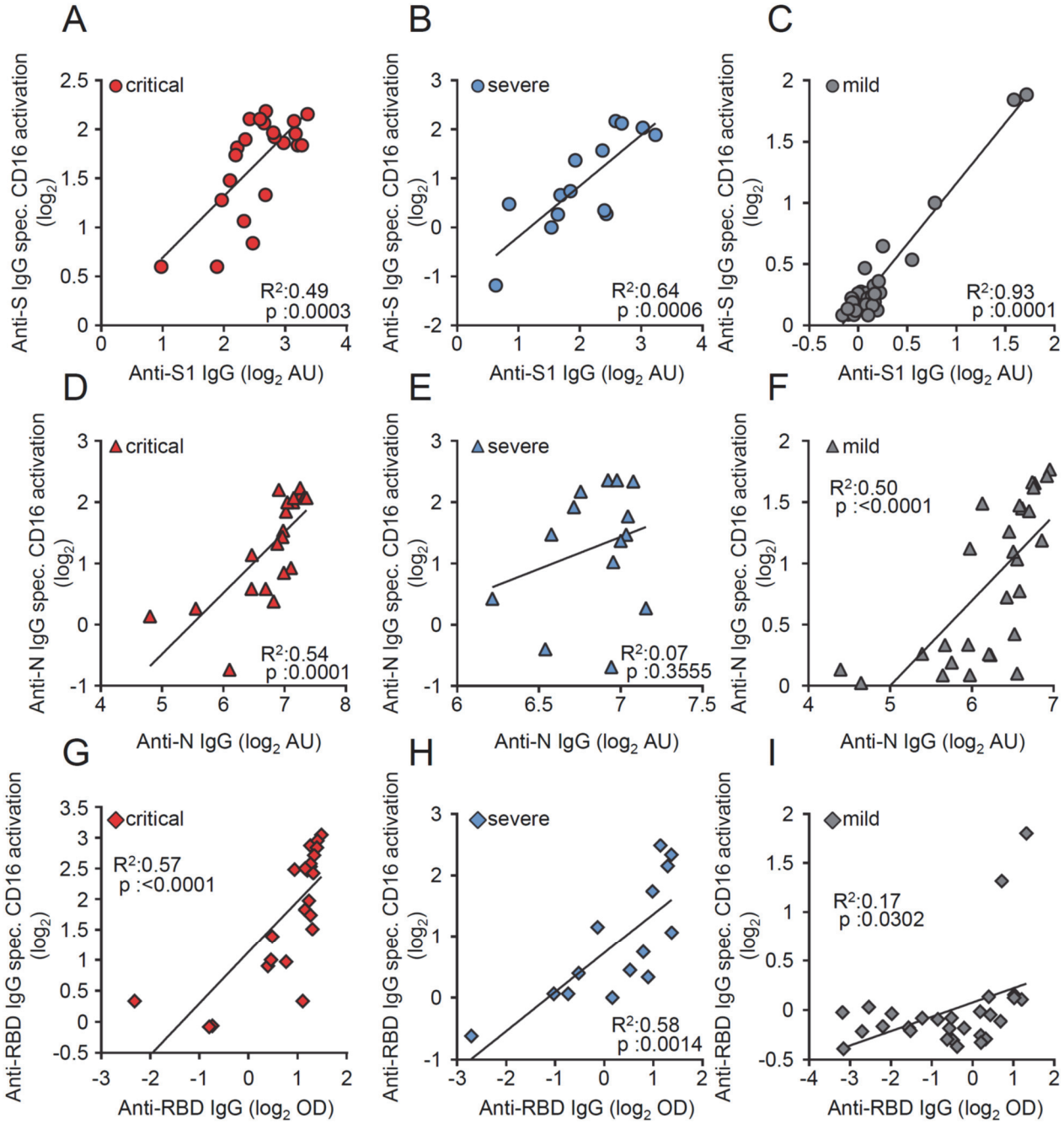

946

947

948 **Figure 3**

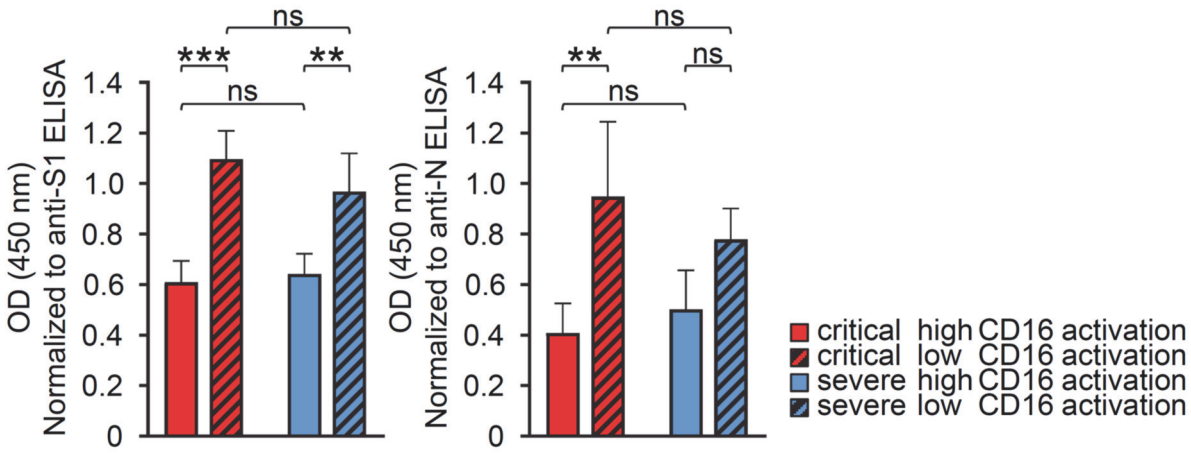

949

950

951 **Figure 4**

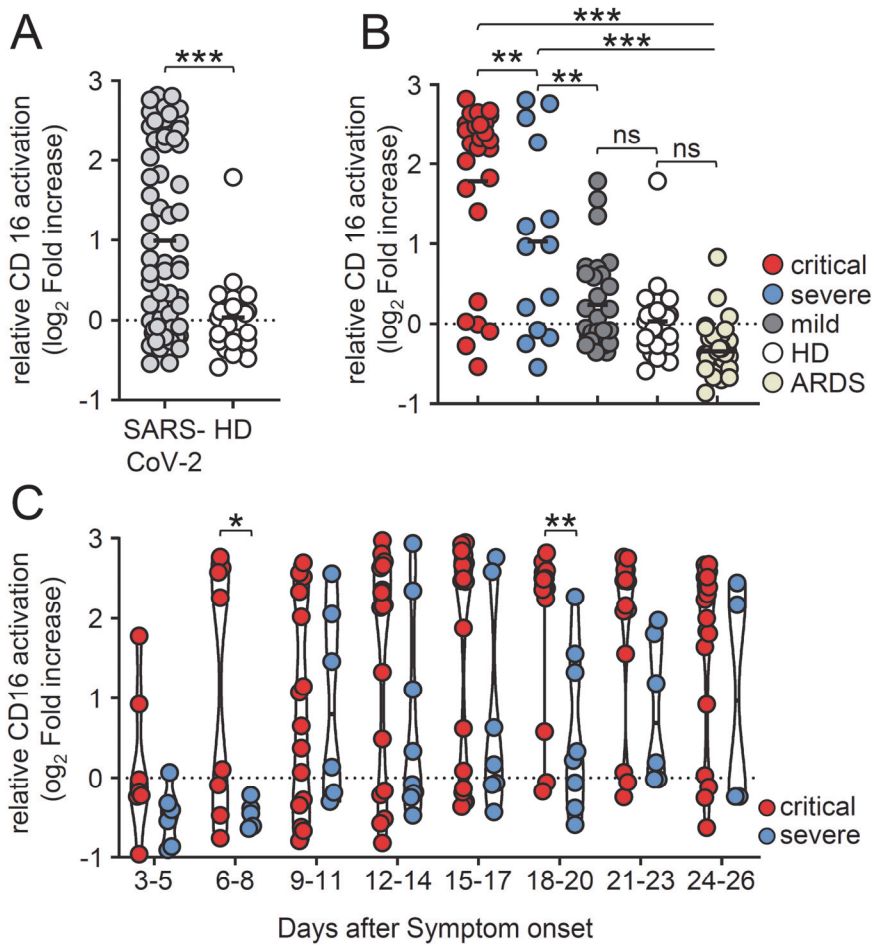

952

953

954 **Figure 4 – figure supplement 1**

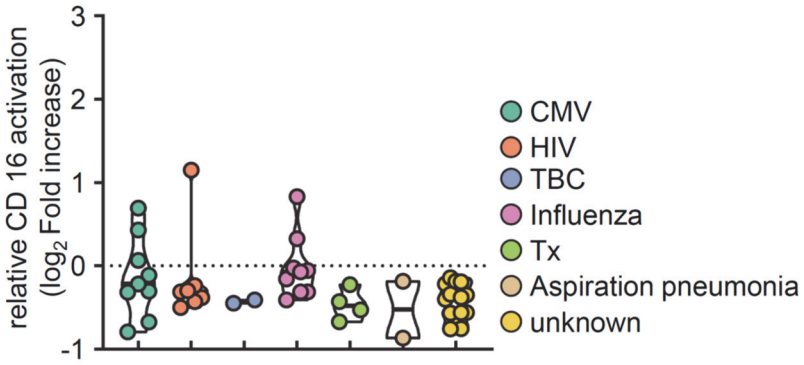

955

956

957 **Figure 4 – figure supplement 2**

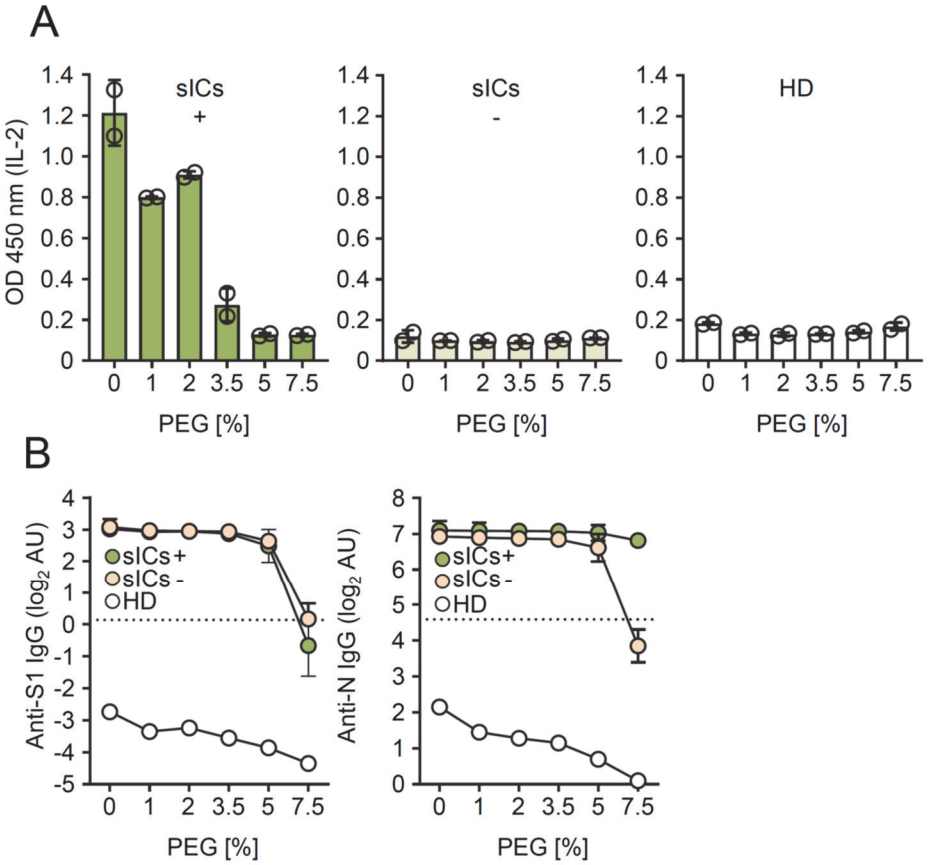

958

Figure 4 – figure supplement 3

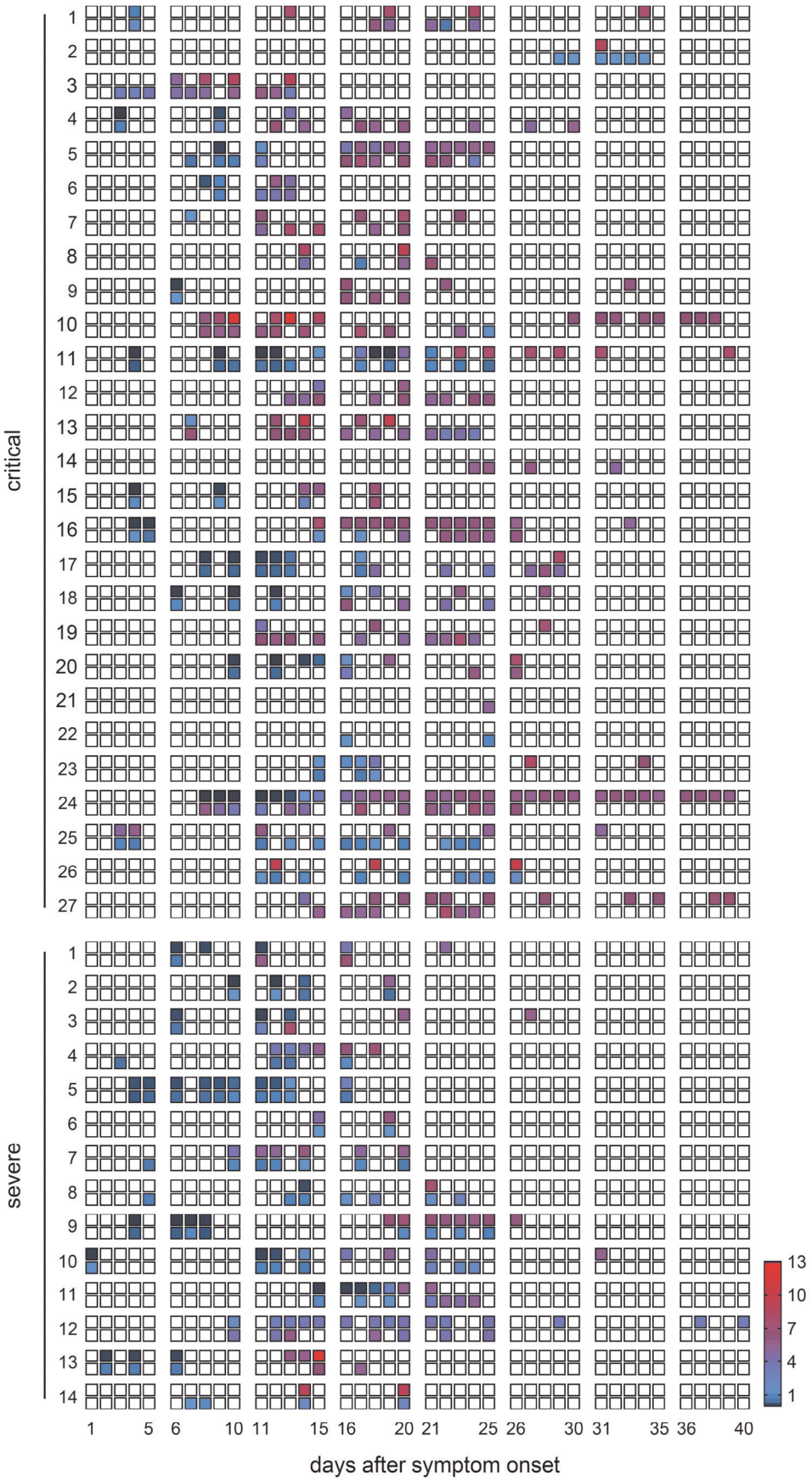

961 **Figure 4 – figure supplement 4**

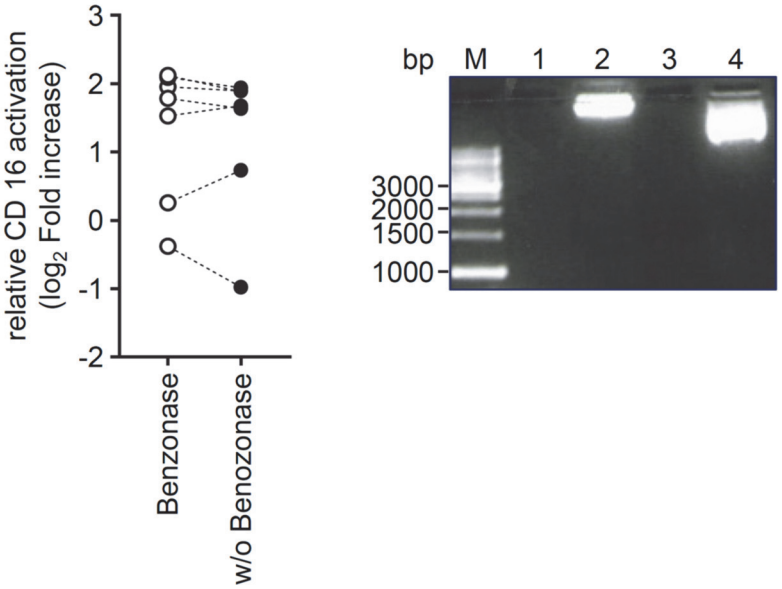

962

963 **Figure 5**

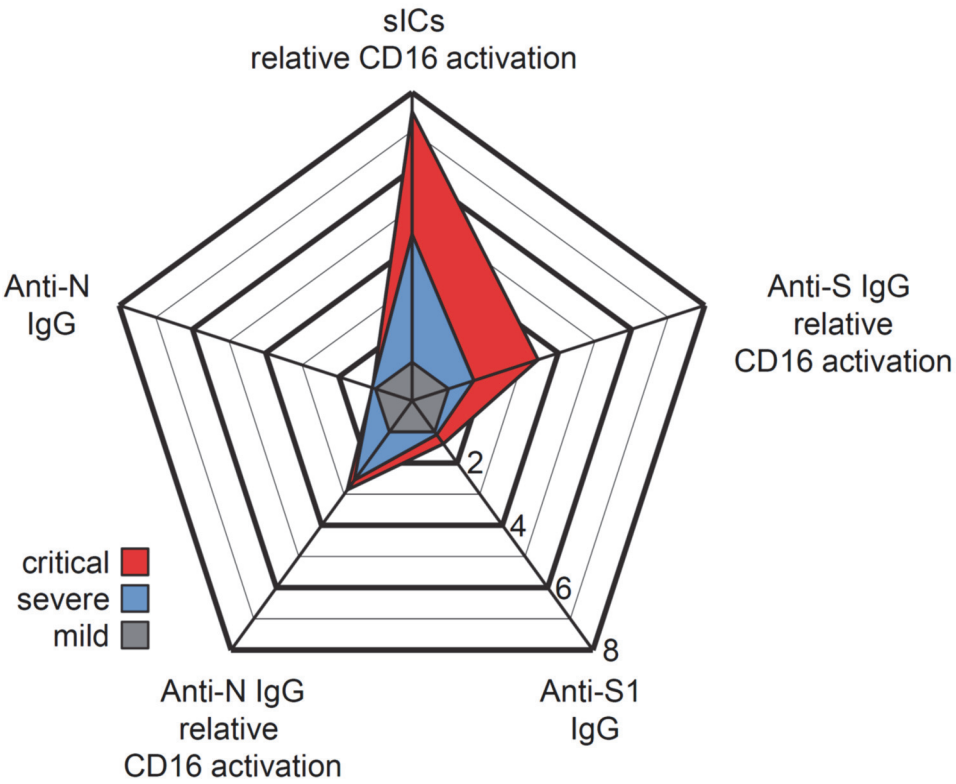

964

965